14

3-D Coupled Basin Reaction, Transport, and Mechanics Modeling: Applications to Fracture, Fault, and Salt Tectonic Regimes

K. Tuncay
Indiana University, Bloomington, Indiana, U.S.A.

A. Park
Indiana University, Bloomington, Indiana, U.S.A.

P. Ortoleva
Indiana University, Bloomington, Indiana, U.S.A.

ABSTRACT

A complex network of coupled reaction, transport, and mechanical (RTM) processes underlies the genesis, dynamics, and characteristics of basins. Estimation of basin evolution is therefore outside the realm of simple approaches. In this chapter, a comprehensive 3-D basin model is described that accounts for a full suite of RTM processes. Our model accounts for rock deformation, fracturing, gouge, and faulting, as well as other processes (multiphase flow, organic and inorganic diagenesis, texture dynamics, and heat transfer). The model accounts for most coupling among these RTM processes and accounts for boundary influences (i.e., the tectonic, sea level, basement heat flux, and sedimentation/erosion histories). Basin RTM provides a platform for integrating available data using the framework provided by the laws of physics and chemistry. It is also being used to test new concepts and models in fundamental basin research.

To illustrate the importance of coupling and comprehensiveness of the model and their 3-D character, we illustrate the use of our model in fractured reservoir, faulting, and salt tectonic regimes. The role of nonlinear phenomena in basin evolution is illustrated.

COUPLED BASIN REACTION, TRANSPORT, AND MECHANICAL PROCESSES

The central role of coupled processes and the related feedback in geologic systems has been demonstrated over the past two decades (see Ortoleva, 1994a, 1994b, for reviews). However, computational and modeling difficulties have restricted basin models to a few processes and to two spatial dimensions. In this chapter, we show that

- mathematical, physicochemical models are now available for a wide range of basin reaction, transport, and mechanical (RTM) processes

- modern, parallelized finite-element codes may address computational issues
- RTM processes may be simulated self-consistently to preserve coupling
- we have developed such a simulator, and it can be used to capture fracturing, faulting, petroleum generation/migration, and salt tectonic phenomena in two and three dimensions

We suggest that only through such a 3-D comprehensive, coupled model can the key E&P problems be addressed.

We present a unique 3-D RTM model, Basin RTM, that utilizes the finite-element solution of equations of rock deformation, fracture network statistical dynamics, rock failure and gouge, multiphase flow, organic and inorganic diagenesis, pressure solution and other compaction mechanisms, and heat transfer. As suggested in Figure 1, all processes in the network of RTM processes are fully coupled and thus are coevolved at all stages of basin history. The RTM equations are solved consistently with the influences at the boundary of the basin (sedimentation/erosion, basement heat flux, climate, sea level, and extension/compression or uplift/subsidence history), as suggested in Figure 2.

The coevolution of all variables is key to making reliable estimations. For example, flow changes fluid pressure, which can cause fracturing and thereby direct fluid flow along preferred fracture directions. Such coupling and coevolution must be accounted for in their full 3-D manifestation. We compute the dynamics of the evolving probability distribution
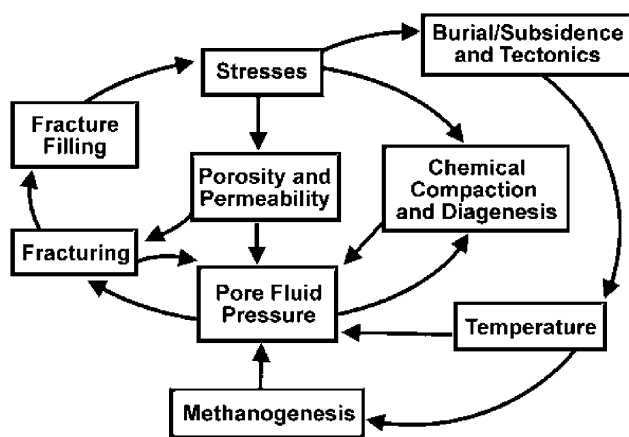

Figure 2. Schematic Basin RTM flowchart showing the interplay of geologic data and the internal RTM processes in evolving a basin over one computational time step.

of fracture length, aperture, and orientation. Rock properties such as the permeability tensor, relative permeability, or rock compressibility are functionals of this probability distribution. These dependencies constitute an essential element of many crustal fluid migrations, rock deformation, and other phenomena. Variables describing rock texture and competency also play a similar role in the coupling of processes.

A key challenge of basin modeling is the need to integrate phenomena on a wide range of space and time scales. In Basin RTM, we describe shorter-scale features (e.g., grains, fluid-phase saturations, fracture network properties) as local variables characterizing the characteristic values within a volume element. Other quantities such as stress, fluid pressure, and temperature are also described in terms of their average value within a volume element. The features we wish to estimate via Basin RTM include reservoirs, compartments, faults, fracture zones, or salt tectonic phenomena. These larger-scale features are defined in terms of the spatial variation across a basin of the microvariables characterizing the aforementioned properties of each finite element. Homogenization is also used to develop coarser descriptions. For example, homogenized (tensorial) permeability represents a finely bedded sequence of sandstone/shale alternation. In these ways, we capture the interplay of spatial scales that are key to the dynamics of a basin.

Figure 1. Complex network of coupled processes underlying the dynamics of a sedimentary basin. These factors and their coupling are accounted for in our unique basin simulator.
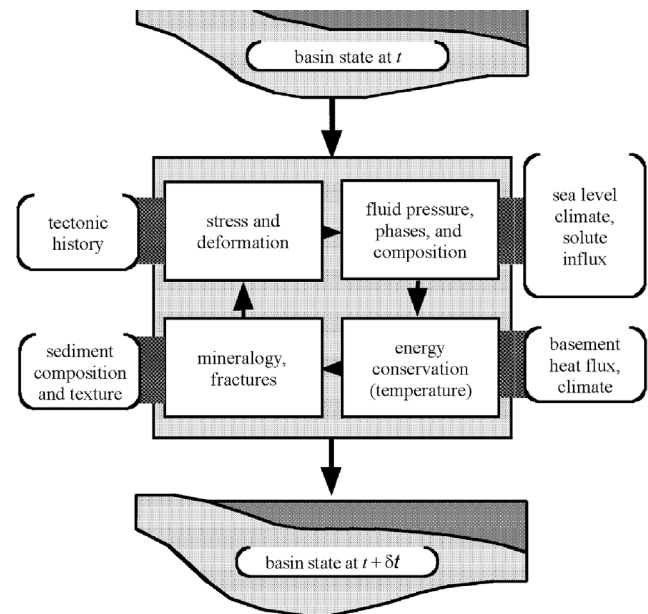
A central feature in our model is the dynamic nature of the texture and its effect on and response to changes in other variables such as stress, fluid properties, and heat transfer. The variables characterizing the fracture network and other texture variables obey ordinary differential equations in a reference frame moving with the velocity of rock deformation. Letting Θ be the collection of texture variables characterizing the fractures and other texture variables, we write

$$\frac{\mathrm{D}\Theta}{\mathrm{D}t} = A(\Theta, \underline{\underline{\sigma}}, f, T) \qquad (1)$$

where $\underline{\underline{\sigma}}$ is stress and f and T are fluid properties (phase and composition) and temperature in each macrovolume element, respectively. In this way, texture couples to stress and other factors. In turn, rock rheology depends on Θ (as well as f and T), completing a stress/deformation $\Longleftrightarrow$ texture feedback. This is just one of the feedback loops contained in Figure 1. Introducing the texture dynamics and the many coupling relations driving the dynamic crustal system is at the heart of our modeling approach (Ortoleva, 1994a, 1994b, 1998; Ortoleva et al., 1987a, 1987b). In the remainder of this chapter, we illustrate the comprehensiveness and capabilities of our approach using examples of fractured reservoirs, fault dynamics, and salt tectonic regimes. In the context of each application, we review and compare our results with those of previous efforts.

Basin modeling has come of age because of the availability of parallel computer hardware, mathematical models, and numeric solution algorithms. Thus, 3-D, multiprocess, fully coupled modeling is a practical tool for petroleum E&P analysis. Finally, we believe that the model we have developed presents itself as the first in this new generation of basin/reservoir models.

BASIN RTM SIMULATOR OVERVIEW

Purpose

Basin RTM is a product of more than 120 man-years of effort in the development of physicochemical models, rate laws, numeric algorithms, visualization, and user interface. At present, Laboratory for Computational Geodynamics (LCG) uses it for its basin research into basin processes and to assist clients in their E&P activities. We expect to release Basin RTM to other academic and industry users in the near future. Basin RTM arises out of the work of Geo-chemical Research Associates (Bloomington, Indiana) and LCG's collaboration with the petroleum industry and the U.S. Department of Energy, the Gas Research Institute, and the U.S. Environmental Protection Agency.

The model we have developed (Ortoleva, 1998; Ortoleva et al., 1997; Tuncay and Ortoleva, 2001; Tuncay et al., 2000a, 2000b; Tuncay et al., 2001) uses variables that describe small-scale features (grain-grain connectivity; local grain size, shape, and mineralogy; porosity; pore fluid composition and phase; fracture characteristics) within each computational subvolume (finite element). These are assumed to vary continuously across the system. Variations of these variables locate and characterize faults and associated fractures, fluid compartments, and other features. Our model shows how these features emerge and change in 3-D by solving partial differential equations for all these variables.

An overview of our Basin RTM simulator is as follows. A complex network of geochemical reactions, fluid and energy transport, and rock mechanical (RTM) processes underlies the genesis, dynamics, and present-day characteristics of petroleum reservoirs or other crustal phenomena in Basin RTM (see Figure 1). Basin RTM integrates most relevant geologic factors and RTM processes that are believed to operate in a sedimentary basin. Because reservoirs are fundamentally 3-D in nature, Basin RTM is based on 3-D finite-element simulation techniques.

The RTM processes and geologic factors accounted for in Basin RTM are outlined in Figure 2. External influences such as sediment input, erosion, sea level, and thermal and tectonic effects are allowed to influence the progress of internal RTM processes. Within the basin, these RTM processes modify the sediment chemically and mechanically to arrive at petroleum and mineral reserves, seals, compartments, faults, and other internal features.

Basin RTM provides a platform for integrating all available geologic data, as suggested in Figure 2, by using the framework provided by the laws of physics and chemistry to facilitate exploration or field development. Available information can be divided into geologic data and physicochemical rate laws. The former makes a simulation tailored to a specific basin. The physicochemical information gives Basin RTM the power to estimate resource location and characteristics and other features of the evolving basin.

Basin RTM can be used to carry out sensitivity analyses or to identify new phenomena such as self-organization and other nonlinear effects that can dramatically affect the disposition of reservoirs in a

basin (Ortoleva, 1990, 1994a). Basin RTM simulations show that the sedimentary basin or other crustal system is highly dynamic, exhibiting a strong degree of autonomy, rather than simply responding to the details of the external influences. Because Basin RTM uses the laws of physics and chemistry to extrapolate data on present-day location and characteristics of lithologies beyond the locations of these data, it enhances the use and interpretation of seismic, well log, surface geologic, and other data in defining the present-day and historic state of the crust. Basin RTM can be used to identify windows of time during which formations along a proposed migration pathway were open and not blocked because of compaction, fracture closure, or diagenetic cementation. Alternatively, Basin RTM can estimate if and when a seal was breached and if hydrocarbons escaped through natural fracturing or through permeability-enhancing diagenetic reactions (see Figures 3–5).

How Basin RTM Works

Basin RTM makes its estimations based on the numeric solution of a set of multiphase, organic and inorganic, reaction-transport equations, and equations of rock deformation and heat transfer. Calculations of all effects are performed self-consistently to preserve crosscouplings between processes (see Figure 1). For example, transport, which is affected by changes of porosity that evolves because of temperature-dependent reaction rates, affects the determination of temperature. Similarly, the rate of kerogen decomposition depends on temperature, which depends
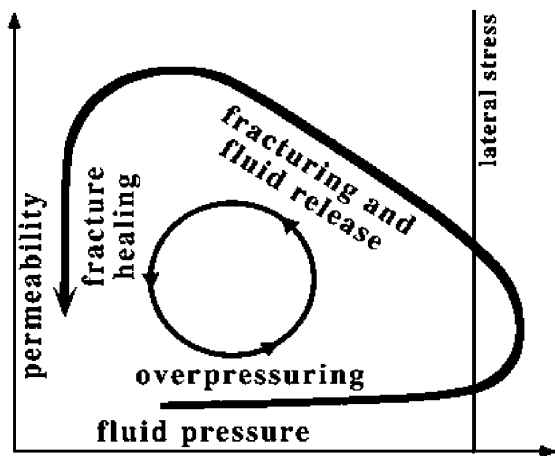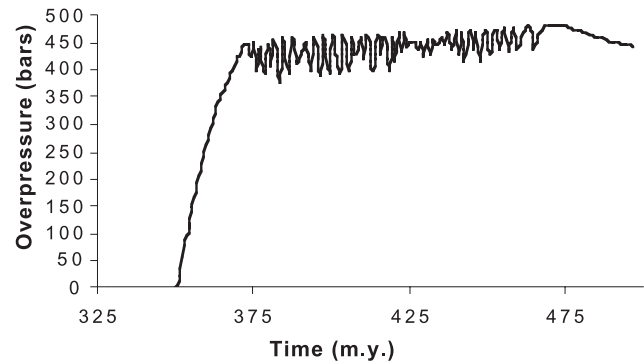

Figure 4. Basin RTM estimated overpressure evolution at the bottom of the Ellenburger Formation. Overpressuring starts at about 350 m.y. into the simulation, when fractures in the layer above the source rock disappear. Oscillatory behavior is a result of cyclic fracturing of the seal driven by petroleum generation. After 470 m.y., the cyclic petroleum expulsion ceases, and the pressure, oil saturation fracturing, and other variables show a more steady behavior (Tuncay et al., 2000a).

on thermal transport that is affected— through fluid buoyancy, thermal conductivity, capillarity, and relative permeability— by the content of organic material and its thermal decay products. All such coupling relations between the full set of RTM processes as in Figure 1 are accounted for in our Basin RTM simulator.

Predictive power is limited for less rigorous approaches that use statistical correlations. For example, in such methods, porosity history is commonly based on a formula relating it or its rate of change to mineralogy and depth of burial. However, porosity evolves because of the detailed stress, fluid composition and pressure, and thermal histories. These histories are different for every basin or part of a basin. Thus, a simple correlation of porosity with depth and lithologic type does not exist in principle. Basin RTM avoids such problems by solving the fully coupled rock deformation, fluid and mineral reaction, fluid transport, and heat transfer problems. Statistical correlations give the average behavior. Because, on the average, there are no interesting features such as producible pools of petroleum, such approaches can have only a limited interest.

The interplay of geologic and physicochemical information in Basin RTM is suggested in Figure 2. Consider one forward time step in a Basin RTM simulation. The purpose of the incremental evolution step is to advance the state of the basin from a time t to a later time $t + \delta t$. Two distinct operations take place simultaneously during this time interval δt. The geologic information is used to (1) fix the input/

Figure 3. Fluid pressuring, fracturing, and fracture healing feedback cycle— one example of the many feedback mechanisms inherent in the RTM process network. This cycle can repeat many times during a basin's evolution when conditions are appropriate.
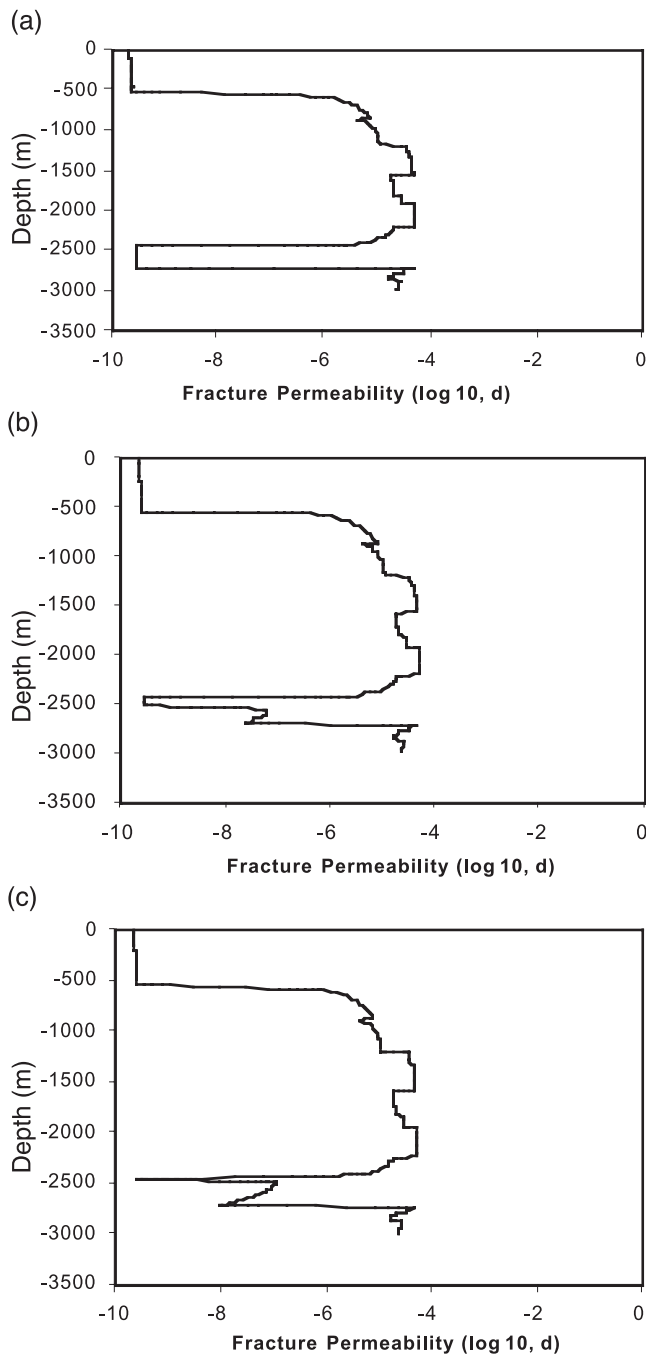
(a)

(b)

(c)

Figure 5. (a), (b), and (c) Fracture permeability profile sequence illustrating the fracture front moving through the seal (between 2450 and 2700 m). Overpressuring of oil and water phases primarily caused by oil generation creates a fracture front moving upward through the seal. Once the overpressure is released, the fractures close, which results in descent of the fracture front, and overpressuring restarts. This cycle continues until the oil generation rate slows down or the seal remains fractured because of tectonic effects. A 2-D fracture front is shown in Figure 11.

output of energy and mass at the basin boundaries and (2) impose the tectonic history (i.e., the overall basin deformation or stress) at the basin boundaries. However, the physicochemical processes are used to determine the evolution in δt of the spatial distribution of the local state. The latter describes stress, fluid properties, mineral content, rock texture, fracture characteristics, and temperature. Secondary properties (permeability, rock rheological parameters, thermal conductivity, and reactive surface area) are computed at each time in terms of these fundamental state variables.

Basin RTM geologic input data are divided into four categories (see Figure 2). The tectonic data change the lateral extent and shape of the basement-sediment interface during δt. These data provide the conditions at the basin boundaries needed to calculate the change in the spatial distribution of stress and rock deformation within the basin. A stress/deformation module that solves equations for incremental stress rock rheology and force balance carries out this latter physicochemical calculation (see Tuncay et al., 2000a, or a brief overview in Appendix A of this chapter).

The next type of Basin RTM geologic data affect the fluid transport, pressure, and composition. These fluid data include sea level changes, basin recharge conditions, and the composition of fluids injected from the ocean, meteoric, and basement sources. The hydrologic and chemical modules use this history of boundary input data to calculate the evolution of the spatial distribution of fluid pressure, fluid composition, and fluid phases within the basin. These physicochemical calculations are based on single or multiphase flow in a porous medium and on fluid-phase molecular species conservation of mass (i.e., the reaction-transport equations). The physicochemical equations draw on internal data banks for permeability–rock texture relations, relative permeability formulas, chemical reaction rate laws, and reaction and phase equilibrium thermodynamics.

The spatial distribution of heat flux imposed at the bottom of the basin is another geologic input/control. These data, as well as the temperature imposed at the top of the sediment pile (i.e., climate and ocean-bottom temperature), are used to evolve the spatial distribution of temperature within the basin during the time interval δt. This evolution is computed using the equations of energy conservation and data for mineral and rock thermal properties (conductivities and specific heats).

The sedimentation data provide the detailed textural characteristics such as grain size, shape, mineralogy,

mode, and organic texture of the sediment being deposited during δt. Basin RTM automatically computes this history by using interpreted well log, seismic, core, and surface data. The physicochemical laws and data are used to calculate the change of the spatial distribution of mineral and organic texture within the basin during δt. These physicochemical calculations involve the rate laws for free face grain chemical kinetics, pressure solution and grain rotation or breakage, grain nucleation, and the laws of kerogen chemical kinetic transformation. The laws of fracture nucleation, extension and aperture dynamics, and the kinetics of cement infilling characterized via a statistical distribution of these variables (Tuncay et al., 2000a, 2000b) are also used.

We use the updated Lagrangian approach to solve the time-dependent large deformation problem for geologic materials satisfying the incremental stress rheology (Bathe, 1996; Bathe et al., 1975; Tuncay et al., 2000a). In our numeric approach, all variables are referred to an updated configuration in each time step. The approach has two major steps. First, the incremental stress rheology equations are solved at the integration points of the finite elements. Second, the displacements are computed by using a global deformation solver. At each time step, iterations of these two steps are performed until the norm of the change in displacements between two consecutive iterations is less than a specified tolerance. The two-step solution technique allows the introduction of new deformation processes with only minor changes in the code. We use the conjugate gradient iterative technique with a simple diagonal preconditioner to solve for the incremental displacements. The finite-element code and iterative solver are parallelized. The details of the finite-element formulation are provided in Tuncay et al. (2000a).

In the multiphase module, the Galerkin-type finite-element approximation is used for saturations, concentrations, and pressures. The nonlinear terms and boundary conditions are treated in a fully implicit manner. An upwinding method is developed and implemented in the multiphase module to stabilize the saturation fronts. The mass matrices are lumped to increase the stability, as suggested in previous studies (Huyakorn et al., 1994; Abriola and Rathfelder, 1993). The computer model accommodates a wide variety of boundary conditions. Because of the highly nonlinear behavior of the equations and the necessity for large time steps, a Newton-Raphson technique is employed to solve the nonlinear algebraic equations arising from the discretization.

The finite-element grid accretes with sediment infilling. A new sediment layer is introduced when the sediment layer at the top of the basin reaches a critical thickness. In contrast, when erosion creates a top layer that is locally too thin, the finite-element grid is locally reorganized to preserve numeric and topographic accuracy. This accreting, reorganizing grid that also adapts to sedimentary features as they are added is required to capture sedimentary detail and to ensure numeric stability and accuracy.

The value of normal stress and the (assumed) absence of tangential shear account for the interaction of the top of the sediment pile with the overlying fluids (atmosphere or sea bottom). The no-shear lateral boundary condition allows for natural compaction at the sides of the basin. Lateral compression/extension and subsidence/upheaval are imposed at the sides and bottom. The sides and bottom are assumed to be impermeable to fluid flow.

All computational modules are packaged in an overall structure that ensures that all equations are satisfied at each time step. The time step dynamically changes to ensure accuracy and computational efficiency. Thus, a time step is short when an ''explosive'' event is taking place and is long during ''sleepier'' epochs.

All these geologic input data and physicochemical calculations are integrated in Basin RTM over many time steps δt to arrive at an estimation of the evolution history and present-day internal state of a basin or field. In this way, the physicochemical laws are used to translate the geologic input data from selected sites into an estimation of the internal state over a basin's history from its inception (or other chosen initial state) to the present. We now illustrate these concepts via several example simulations. In the appendices, we consider aspects of rock rheology used in Basin RTM in more detail. All computations are carried out using parallelized algorithms to solve the finite-element equations on a multiprocessor hardware platform.

FRACTURES, FAULTS, AND BASIN DEFORMATION

Basin RTM can be used to estimate the location and characteristics of fracture zones and the structure of fault zones. The Basin RTM fracture model accounts for the statistics of fracture orientation,

length, and aperture (see Tuncay et al., 2000b, or a brief overview in Appendix C of this chapter) and thereby accounts for the following:

- fracture orientation reflecting the 3-D stress tensor
- new fractures are added to the evolving network as the stress tensor and fluid pressure change because of tectonics or diagenetic changes in rheology
- the fracture network characteristics affect the tensorial fluid transport (e.g., permeability) and rock rheological parameters
- the model allows for the construction of rose diagrams and other parameters that can be compared with observation
- the model accounts for the mineralogy, texture, and statistical variations of properties (notably weak spots) that affect fracture density

To model fractures and faults in a reservoir or basin, one must carefully consider scale. For modeling fractures of meter length and submillimeter aperture in such large domains, it is not feasible to introduce a submillimeter numeric grid across the system. To solve this problem, we introduce the probability of local fracture length, aperture, and orientation. For the present problem, by definition, a macrovolume element is smaller than the scale of the phenomenon of interest (a reservoir) but large enough to contain a statistically significant number of fractures. Such a theory is thus, by nature, a statistical model with the macrovolume element being the sampling volume.

In Basin RTM, a fault is described as a spatially localized disturbance in the spatial profile of rock competency, gouge, and fracture network statistics. Several such features can be spontaneously generated within the basin. Because several finite elements in spatial directions normal to the overall fault plane are needed to resolve a fault, the number of subfaults or other zones that can be simulated within a basin is clearly limited to 5–100, depending on CPU availability. In addition, the nature of our modeling concepts limits the spatial distance to which we resolve features. For example, we describe fractures in terms of the statistical distribution of length, aperture, and orientation within a finite element. Clearly, we cannot thereby capture only length scales greater than the mean fracture spacing. Thus, a fault is envisioned as a roughly planar disturbance in the fracture statistics, rock competency, and gouge variables simulated by Basin RTM. Finally, Basin RTM does not presently have a dual porosity/permeability model for the fracture system so that fracture-related flows are presently characterized in terms of the effect of a lumped (fracture plus matrix) permeability.

Because of its importance to both petroleum and geologic sciences, many researchers have studied fracturing (see Pollard and Aydin, 1988, and Lorenz et al., 1991, for reviews). Associated extensional stresses commonly explain fractures in areas subjected to bending (Friedman, 1976). The existence of fractures in near-horizontal layers has been attributed to unloading (Currie and Nwachukwu, 1974; Engelder, 1987), high fluid pressure (Pollard and Aydin, 1988; Ortoleva, 1998) and to anisotropic stress that is influenced by nearby geologic structures (Segall and Pollard, 1983; Currie and Nwachukwu, 1974). We believe that a combination of the effects listed above causes fracturing in near-horizontal or folded areas. If the local fracture kinetics is well described by fracture growth/healing laws, a multiprocess deformation model coupled to fluid flow and fracturing can be used to quantify the relative importance of these effects.

It is well documented that fracturing strongly depends on lithology (Segall and Pollard, 1983; Lorenz et al., 1991; Fischer et al., 1995; Gross, 1993; Wu and Pollard, 1995; Hancock et al., 1984; Kulander et al., 1979). Although fractures can occur in almost any type of rock, they are more common in brittle rocks (Mallory, 1977). Furthermore, fractures in a brittle lithology commonly discontinue at the interface of more ductile lithologies (Engelder and Geiser, 1980). Another observation is that fracture spacing is strongly dependent on bed thickness and lithology (Fischer et al., 1995; Wu and Pollard, 1995; Gross, 1993; Nickelsen and Hough, 1967; Harris et al., 1960). However, a simple correlation between fracturing and bed thickness does not seem feasible because of the many factors operating, such as fluid pressure, state of stress, neighboring lithology properties, and tectonics.

There is a vast amount of work on approximations for the permeability of fracture networks (for example, Koudina et al., 1998; Oda, 1986; Long and Billaux, 1987; Berkowitz, 1995; Odling, 1992). However, in these studies, a fracture network is generated either by an independent (decoupled) statistical geometric model or based on data. Here, we address the evolution of a 3-D complex fracture network based on fracture growth and initiation laws proposed earlier (Segall, 1984; Atkinson, 1984; Dutton, 1974; Wang et al., 1983; Sonnenthal and Ortoleva, 1994; Brantley et al., 1990).

Fracture-mediated petroleum expulsion, migration, and escape from reservoirs are key aspects of the dynamic petroleum system (Figures 3–5). In most of the existing basin evolution models, it is assumed that rocks fracture when fluid pressure exceeds a specified fraction of lithostatic stress (Maubeuge and Lerche, 1993, 1994; Roberts and Nunn, 1995; Wang and Xie, 1998). This assumption ignores the dependence of fracturing on lithologic properties and lateral basin tectonics. In Basin RTM simulations, we find that fracturing strongly depends on rock composition and texture, including mineralogy, grain size, and porosity, which indirectly affect the stress tensor (Figures 6 and 7). Another limiting assumption of these models is that there exists a simple dependence of porosity on effective stress (Maubeuge and Lerche, 1993, 1994; Roberts and Nunn, 1995; Wang and Xie, 1998; Ungerer et al., 1990; Schneider et al., 1996; Luo and Vasseur, 1996). This results in a very smooth porosity profile that misses the influence of porosity on rock composition and texture. In our approach, porosity is obtained by solving the mass balance equation for solids and computing rock deformation velocity using a multiprocess, incremental stress rheology that contains the elastic and viscous parameters, which are functions of texture and composition. By coupling mass balance algorithms with our porosity
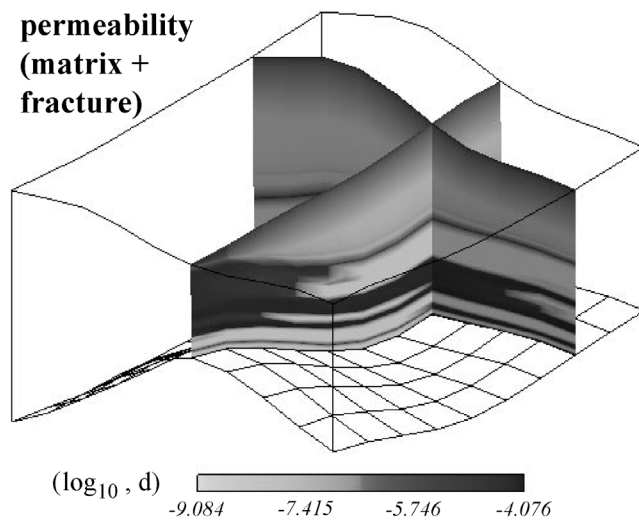

Figure 6. Estimated cross sections of permeability at 45 Ma from a simulation of Piceance Basin, Colorado. The system is 50 × 48 km wide and 1–3 km deep. Different permeabilities reflect varying sediment compositions, including porosity, texture, mineral grain sizes, and fractures.
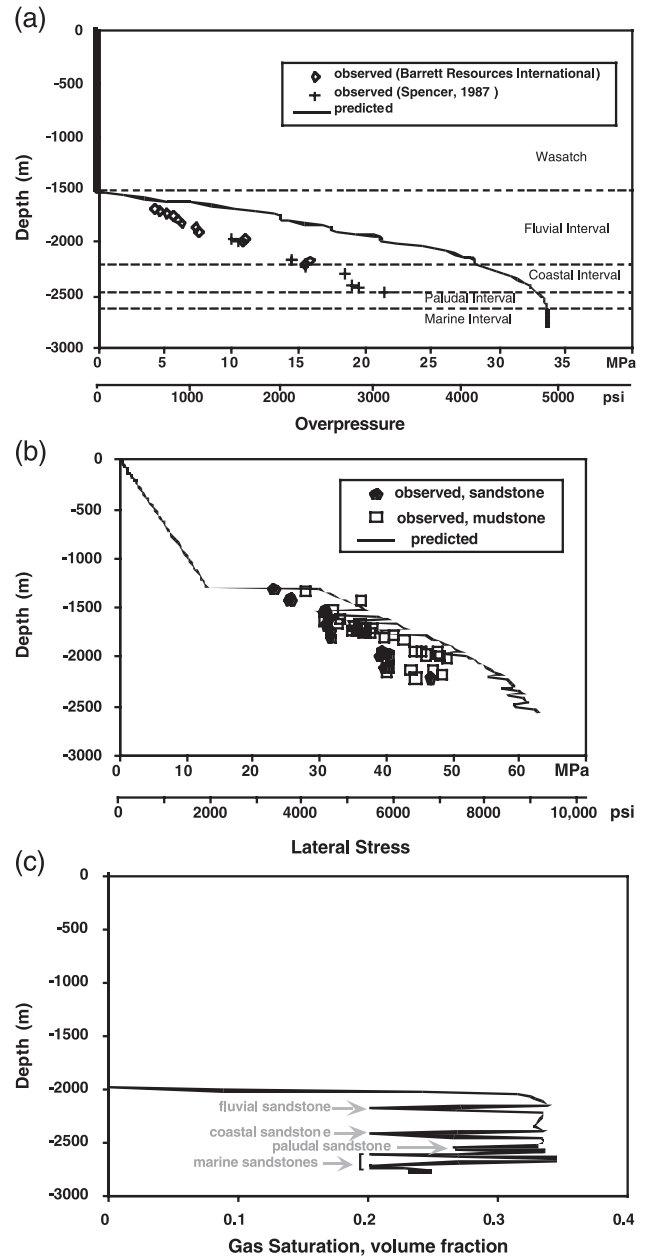

Figure 7. Simulations by Basin RTM show good agreement with observations. Present-day fluid pressure (a) and least compressive stress at the MWX site, Piceance Basin, Colorado, compared with observations, are shown. In sandstones, the lateral stress and fluid pressures are found to be similar, indicating their vulnerability to fracturing, whereas in mudstones, lateral stress exceeds fluid pressure, underscoring the lack of fracturing in them at present day (as observed). Our estimations also show that this situation is dynamic— during an epoch in the past, some of the mudstones were also fractured in some areas in the Piceance Basin, as suggested in the literature. (c) Estimated natural gas saturation (from Payne et al., 2000).

and stress solvers, porosity and stress are computed self-consistently. Consequently, shales are commonly estimated to have lower porosity and higher least compressive stress than sandstones (Figure 7). The small grain size combined with low porosity results in very low permeability, and thus, these layers can form efficient seals. Furthermore, our Basin RTM results show that low shear viscosity/bulk viscosity ratio makes fracturing very unlikely in the absence of flexure or extreme overpressuring mechanisms such as petroleum generation or fluid thermal expansion.

In other basin evolution simulators, fracture permeability is assumed to be isotropic. These more simplified models cannot accurately describe fracture orientations, the full stress tensor, or irreversible (e.g., viscouslike rather than poroelastic) behavior (Figure 8). The interaction between the deformation/stress computation and fracturing is also disregarded in simpler models. Rocks fracture because of the difference between fluid pressure and least compressive stress. As fractures open, overall rock volume increases and fluid pressure in the fractures compresses the rock, increasing the compressive stress normal to the fracture plane. Thus, fracturing is a self-limiting process. Therefore, as fractures open, they provide a pathway for fluid escape, and second, the volumetric strain caused by fractures increases the confining stress that reduces the rate of fracture growth (Tuncay et al., 2000a, 2000b).

Although 1-D and 2-D studies give hints about the dynamics of basin evolution, a 3-D basin simulator is necessary to take 3-D geometric effects into account (Figures 6 and 9–11), as well as the complexity of the coupling of stress tensor components implied in force balance and rock rheology. This becomes extremely important where flexure and the direction of tectonic compression/extension that may change during the basin's history influence fracturing. Figure 11 shows a 2-D fracture front taken from a Basin RTM simulation of Andector Field, west Texas.
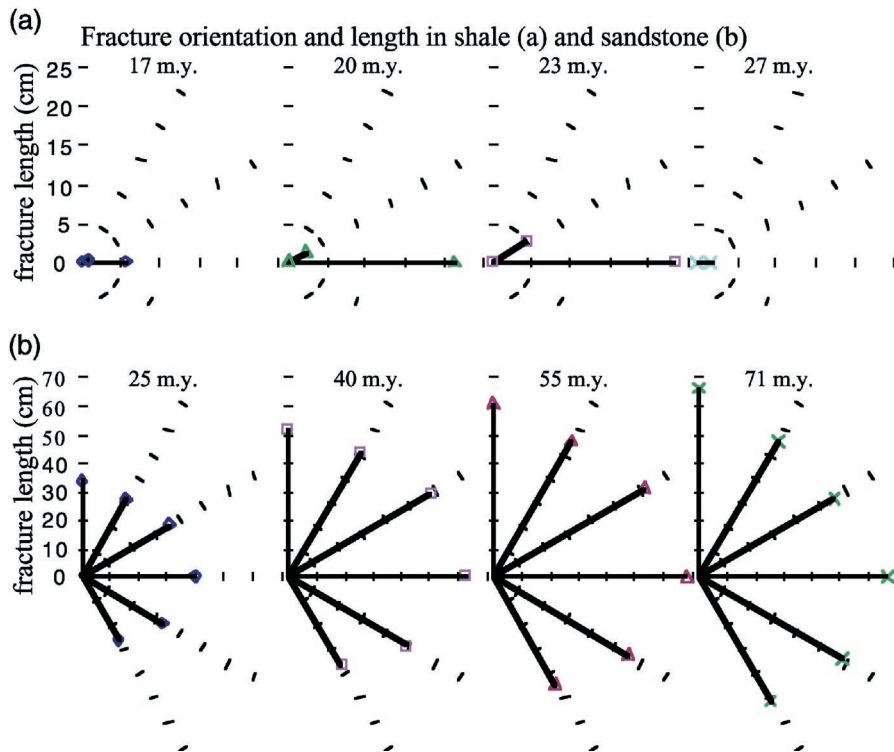
Although the history of temperature, sedimentation rate, and subsidence rate is among the most important parameters that affect the evolution of a basin, some basin simulators start with a predefined grid (Schneider et al., 1996). In other words, two basins with the same final thickness and lithology but different histories of these factors are assumed to behave similarly. This approach ignores the time dependence of, for example, overpressuring, which commonly correlates with sedimentation rate and is a key factor in fracturing as well as deformation (Wang and Xie, 1998; Ortoleva, 1994a).

Another limitation of previous models is the omission of shear failure and fault dynamics. Only a few models consider the contribution of mechanical shear to rock failure (Luo et al., 1998; Larson et al., 1993). However, these models are limited to two dimensions. In Basin RTM, a Drucker-Prager-type failure function is used to signal shear failure via a transition in rock viscosity. To estimate

Figure 8. Predicted fracture orientations and length in a shale (a) and a sandstone (b) from the Piceance Basin. Changing sediment properties, stress, and fluid pressure during the evolution of the basin result in dynamic fracture patterns, which significantly affect the anisotropy of fracture permeability. If the enhanced permeability from fracturing is significant, it can direct the flow of petroleum. Understanding such occurrences of the past, therefore, can be important for identifying or understanding reservoirs in presently unlikely structural and stratigraphic locations.
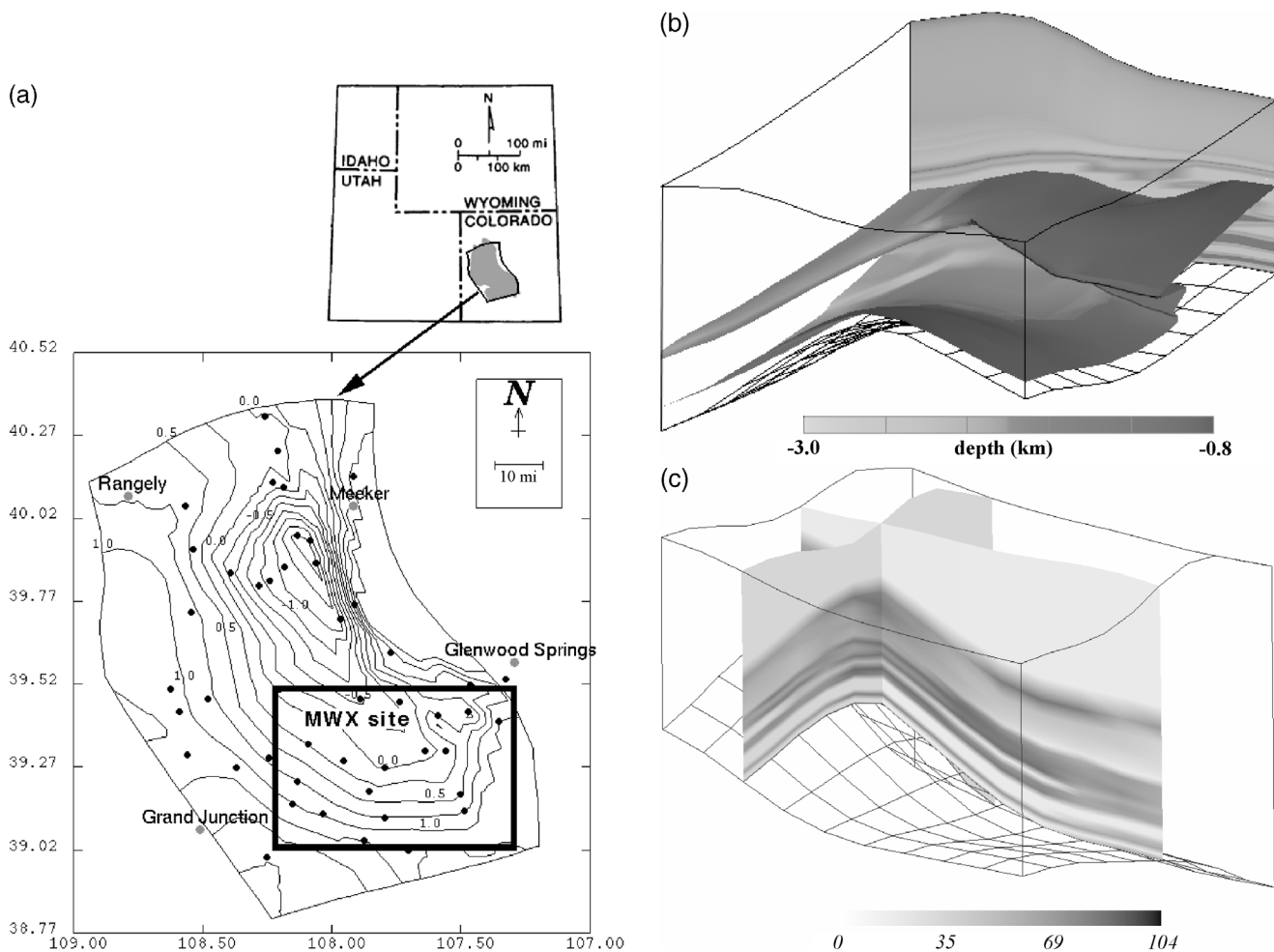
Figure 9. (a) Simulation domains for basin-scale and interfield studies (thickly outlined box). The Rulison Field is shown in the upper northwestern area of the latter box. (b) Isosurface of overpressure (15 bars) toned with depth. The folded, multilayered structure is dictated by the interplay of lithologic differences and fracturing and shows the 3-D complexity of conductivity of overpressured zones. Thus, stacked overpressured compartments as viewed as a simple pressure-depth curve may hold little insight into the full three-dimensionality of the structure. (c) The distribution of fracture length reflects lithologic variation and the topography imposed by the basement tectonics. The layered fracture length structure is closely related to the layering in overpressure surface (from Tuncay et al., 2000a; reprinted with permission from Elsevier).

faulting and other rock failure phenomena, we introduce a model that accounts for rock competency (Γ) dynamics (see a brief review in Appendix B of this chapter or in Tuncay et al., 2001). Let $\Gamma (0 \leq \Gamma \leq 1)$ be the fraction of grain surface area that is attached to neighboring grains. Large Γ implies competency, whereas in a low-Γ rock, there are few intact grain-grain contacts and the effective viscosity is low. Rheological quantities such as rock strength or viscosity are strongly dependent on Γ in Basin RTM. This feature extends the applicability of Basin RTM to fault formation problems (Figure 12). We have already included the rate of strain caused by gouge (Figure 13) to show the effect of shearing on

the particle size distribution and porosity (Ozkan and Ortoleva, 2000; Ozkan et al., 1998).

Our results on geologic phenomena involving patterns from oscillatory intracrystalline zoning, dissolution fingering, and metamorphic layering to sedimentary basin compartmentation have shown that such regular and chaotic spatiotemporal complexity can emerge spontaneously— i.e., without the need for an externally imposed oscillatory influence (for a review of our work, see Ortoleva, 1994a, 1994b, 1998). All these studies show that these phenomena occur spontaneously because of the operation of coupled, nonlinear processes and a continuous source of energy. Thus, major and minor seismic oscillatory
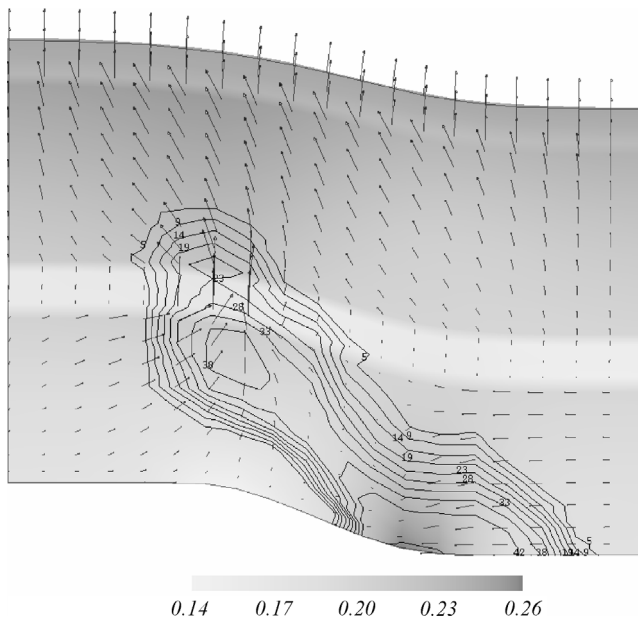
Figure 10. Cross section of a 2-D, 5- × 2.5-km normal fault system after 5 m.y. of simulation. The shading indicates porosity and shows differences among the four lithologies; the shales (low porosity) are at the middle and top of the domain. Higher porosity regions (in the lower right and upper left corners) and the fracture length (contour lines) arose because of the deformation created by differential subsidence. Both stress field and fracturing are strongly affected by rock composition and texture. The arrows indicate fluid flow toward the region of increasing porosity (lower right) and through the most extensively fractured shale.

2000a, 2000b; Ortoleva, 1994a, 1998) (see Appendix A of this chapter).

SALT TECTONIC REGIMES

Background

Salt movement in the subsurface can dramatically affect the distribution and character of fracture zones, petroleum pools, faults, and other features for several reasons:

- Salt diapirism and related phenomena can cause flexure and otherwise can dramatically affect the stress regime in the neighboring sediments.
- Salt movement can affect the topography of the seafloor and thereby the geometry and lithologic character of the salt-adjusted sediments.
- Salt is of vanishingly small permeability and therefore can isolate high overpressure (up to lithostatic levels) and thereby influence effective stress in the underlying sediments.
- By distorting the heat flux, changing the salinity, and altering the permeability and other fluid flow patterns, salt can change the diagenetic history and rock mechanical properties.

Because salt withdrawal is believed to be an important factor in fracturing and faulting in some areas, we have incorporated advanced salt tectonics
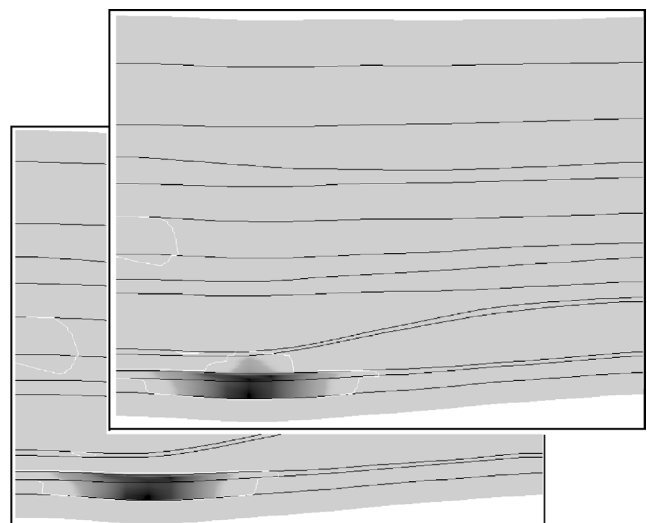
behavior occurs spontaneously in response to steady overall plate motion and heat and mass flux from deep within the mantle. Therefore, seismicity is self-organized, not imposed.

Our model accounts for the changing rock rheological parameters that accompany the changing lithologic and fracture properties. The bulk, shear, and effective stress coefficients of the (assumed) isotropic rocks are computed using Berryman's (1980, 1986) composite medium theory modified for the presence of fractures (Budiansky and O'Connell, 1976; O'Connell and Budiansky, 1977). In our approach, by assuming that viscosities and other rheological parameters depend on Γ and other texture variables, rheology is computed as a function of the instantaneous mechanically and diagenetically modified texture. With this, evolving rheological properties are used to compute stress and deformation using an incremental stress rheology (Zienkiewicz and Cormeau, 1974; Rice, 1975) that is extended by the authors (Tuncay et al.,

Figure 11. Cross sections from Andector Field, west Texas. The black lines show lithology contacts, whereas the white lines show the fracture zones. The fracture length is represented by gray tones. Note the fracture front moving upward. Fracturing is caused by the combined effects of overpressuring and flexure.
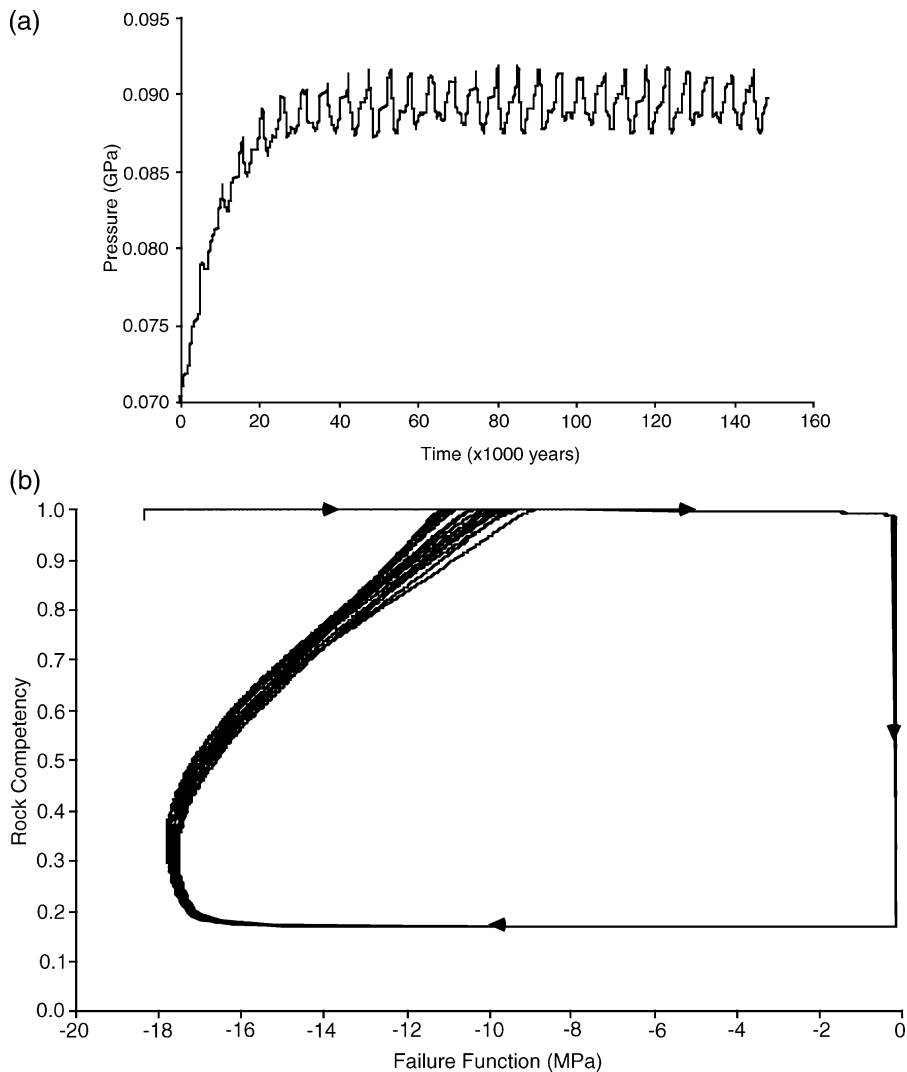
(a)

(b)

Figure 12. (a) Evolution of intrafault fluid pressure to a harmonic fluid influx rate; (b) trajectory on failure function–rock competency plane. Fluid influx from ductile roots of faults significantly affects the rock strength (Rice, 1992). Because porosity, fluid pressure, and stress components are tightly coupled through RTM processes, a disturbance in one of the variables is reflected in other variables. The high-frequency oscillation in fluid pressure is caused by volumetric changes during slip events.

modeling into Basin RTM by calibrating our rheology to capture salt deformation experiments.

With this, Basin RTM can address the following E&P analysis challenges:

- estimate the location and geometry of faults or fracture zones that were created by salt motion
- estimate the morphology of sedimentary bodies that were created by salt deformation
- estimate overpressure and subsalt reservoirs
- estimate the velocity of salt deformation to avoid pipeline and platform damage

- locate pools of petroleum or migration pathways that were created by salt tectonics
- assist in the interpretation of seismic data in salt tectonic regimes

The interplay of salt deformation with the rheology of the surrounding strata is key to understanding the salt deformation ⟺ reservoir location and characteristics relationship. Salt movement, overall tectonics, and overpressuring induce the continuous and discontinuous (i.e., faulting and fracturing) responses of the surrounding sediments. In turn, the deformation of these sediments promotes or inhibits salt motion. Thus, salt bodies and their adjacent sediments constitute a strongly coupled system.

It is believed that the coupling between salt-motion-induced sediment topography and the distribution of sedimentation is key to determining salt and neighboring sediment body geometries. We suggest that this dynamic results in self-organization (Tuncay and Ortoleva, 2001). If a rising diapir causes a bump in the seafloor, additional sediment will tend to deposit on the flanks of the bump. This sediment will tend to squeeze more of the (relatively light) salt into the diapir, causing it to rise further. If this dynamic continues, the diapir will have self-sustained growth (see Figure 14). If the tip of the salt diapir is too far below the surface of the sediment, this coupling is diminished, so that there is a limited depth range for the operation of this mechanism.

The general theme is as follows. The distribution of sedimentation rate is a function of the shape of the top of the sediment pile. The local sedimentation rate determines the local overburden on the salt and hence promotes salt withdrawal and its injection into the diapir. If the salt and sediment are both perfectly horizontal, this feedback is not operating. However, even the smallest departure from planarity
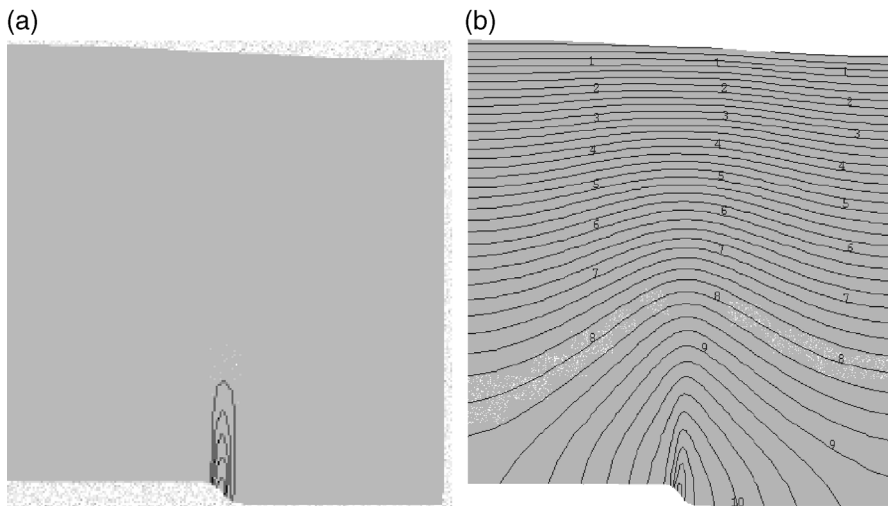
(a)

(b)

Figure 13. The effect of gouge on (a) porosity and (b) overpressure. The size of the domain is 3 × 3 km in cross section. The fault width is 0.1 km and the rate of faulting is 0.2 km/m.y. To isolate the effect of gouge on the pressure and texture, a very high bulk viscosity is used. Therefore, the only overpressuring mechanism present is the gouge-related changes in the texture.

can trigger diapirism. Some caution is required, however, in that there may be a critical amplitude below which there is no diapiric response. Whether through small or large finite amplitude instability, diapirism emerges as a symmetry-breaking instability of the horizontal, planar state, a theme common to other patterning phenomena in chemical and physical systems (Nicolis and Prigogine, 1977; Ortoleva, 1992) and geologic systems (Haase et al., 1980; Nicolis and Nicolis, 1987; Ortoleva et al., 1987a; Ortoleva et al., 1987b; Ortoleva, 1990).

The specific algorithm used in our simulator is as follows. The system is fed a spatial average amount of sediment per year (for example, 200 m/m.y. of alternating equally thick shale and sandstone precursor sediments). However, the local rate of sedimentation is computed in a given computational time step to eliminate any putative departure from planarity of the topography that is induced by the diapirism and salt withdrawal (at the flanks of a diapir). Consequently, minibasins or other sediment accumulation are created.

The sedimentation ⟺ salt deformation dynamic is just one of a family of feedback processes operating in a salt tectonic province. Buoyancy of salt relative to compacted sediment also can drive a patterning phenomenon analogous to the Benard instability, wherein overturning convection can emerge where a denser fluid overlies a lighter one (Biot, 1966; Biot and Ode, 1965; Nicolis, 1995). The

complex rheology of the rocks surrounding a salt body may mask the pattern-forming process, however. For example, where horizontal salt/sediment layers are subject to an overall lateral extension, the pattern of locally induced failure in the overlying sediment can promote upward migration pathways for the salt that was otherwise trapped by the overlying competent and stiff layer of sediment. Similarly, salt diapirism can result from its complex interplay with buckling and failure instabilities, as in a regime of lateral compression.

An overall sloping of the salt layer or an overall gradient in the rate of sedimentation (as from near offshore to farther in the Gulf of Mexico) can trigger salt diapirism. These larger spatial-scale ''perturbations'' of the ''perfect'' horizontal state can result in arrays of salt diapirs and other features on a much shorter scale. Such wavelength selection (i.e., the appearance of patterns on scales larger or smaller than that of the perturbation) is common in nonlinear dynamic systems. Such
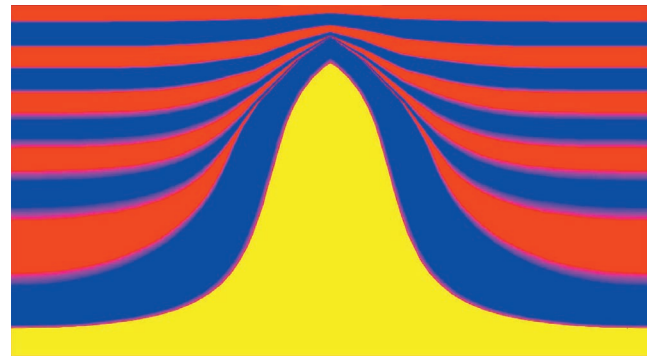
Figure 14. Basin RTM simulated salt wave showing associated deformation (as indicated by the shape of the evolved salt body). The state after 8 m.y. of deformation and sedimentation is shown. The salt bed originally had only a 400-m topographic contrast. Alternating layers of sandstones and shales above the salt are present at this stage. The salt tectonic ⟺ sedimentation interaction induced the sediment geometry and the generation of minibasins at the flanks of the wave (Tuncay and Ortoleva, 2001a).

preferred scales of diapirism correspond with the size of salt minibasins and in the spacing of salt waves emerging in a sloped salt bed.

Other Experimental and Numeric Studies

Although there is a vast number of observations of salt structures (Jackson and Talbot, 1986; Seni and Jackson, 1984; Cobbold, 1993) and experimental studies on salt rheology (Aubertin et al., 1994; De Las Cuevas, 1997; Carter et al., 1993; Mazariegos et al., 1996; Van Keken et al., 1993; Munson and Dawson, 1984), there are only a few attempts to numerically simulate them. Moreover, previous simulators are 2-D, and both salt and sediment are treated as bulk materials, i.e., fluid flow through the pores, and its influence on effective stress is ignored. None of these models accounts for the evolving rheology of the sediments caused by diagenesis and mechanical processes, petroleum generation, and the changing thermal regime. Therefore, existing salt tectonics simulators do not have the comprehensiveness needed for E&P analysis in tectonic regimes.

Daudre and Cloetingh (1994) presented a 2-D analysis based on Stokes flow. In this approach, both sediment and salt are treated as nonlinear viscous fluids. A Drucker-Prager criterion is adopted to model the inception of brittle deformation. The density of sediment was calculated based on a pressure-dependent porosity. An updated Lagrangian formulation was used to simulate large deformations. They showed that extension combined with salt rheology favors salt diapirism. Van Keken et al. (1993) obtained the effective rock salt viscosity by adding dislocation creep and pressure solution creep. The effective salt viscosity was allowed to depend on temperature, strain rate, and grain size. Pressure solution dominated the salt motion. Sediment density was taken as a function of depth. With these assumptions, they performed a sensitivity analysis for the effect of overlying sediment viscosity. Their results showed that the sediment viscosity/salt viscosity ratio is an important factor in determining salt motion and geometry. Mazariegos et al. (1996) developed another 2-D model based on Stokes flow. They used two different salt rheologies: a dislocation-creep power law and a fluid-assisted creep law. The functional form of the salt rheology depended on grain size. Although Mazariegos et al. (1996) used a rather complex rheology for salt, sediment viscosity was taken to be constant. They showed that their fluid-assisted creep law results in faster salt

motion. They concluded that a better understanding of salt diapirism requires a better characterization of surrounding rock rheology. Schultz-Ela et al. (1994), who used the commercial program GEOSIM-2D for their numeric modeling, presented a 2-D study. Salt was treated as a viscoelastic material, whereas sediment was modeled with an elastoplastic rheology. Plastic yield was determined with a Drucker-Prager criterion.

The differences between Basin RTM and those mentioned above are as follows.

- *Concept of composite media*: In our approach, in contrast to previous studies, the descriptive variables of all solid and fluid phases (stress, velocity, concentrations, etc.) and variables describing the texture of the porous medium (i.e., volume fractions, mineralogy, grain size, and porosity) are coevolved via RTM equations accounting for interactions and interdependencies between them.
- *Incremental stress rheology*: Our incremental stress rheology integrates poroelasticity, viscous flow with yield behavior, fracturing, and pressure solution. In most studies, salt and sediment are considered as nonlinear Newtonian fluids ignoring the effects of elasticity and fracturing (Ortoleva, 1994a, 1998; Ortoleva et al., 1997; Tuncay et al., 2000a, 2000b).
- *Faulting*: We use the Drucker-Prager criterion to signal failure and evaluate the rheological properties of the failed medium. However, the nonlinear shear viscosity is obtained from coevolving texture variables such as rock competency, mineral composition, grain-size distribution, and porosity. In our model, competency of a rock is a measure of the integration of grain-grain contacts. It has memory, i.e., it depends on the history of failure through its determination as the solution of a time-differential equation (Tuncay et al., 2001).
- *3-D fracture network dynamics*: We have developed a 3-D fracture mechanics model based on the stress tensor, fluid pressure, and rock texture variables. Because previous models are limited to simulate the behavior of bulk materials, they cannot be used to estimate or understand tensile fractures that contribute to the tensorial rock permeability (Tuncay et al., 2000b).
- *Single and multiphase flow*: To understand the interplay of salt motion and fluid migration, salt deformation and fluid flow should be solved

simultaneously. The presence of seals and over-pressured and underpressured compartments can enhance or suppress salt motion, an effect that is not accounted for in other models.

- *Oil and gas generation*: As a natural consequence of the availability of our multiphase flow solver, generation and migration of petroleum can be studied in association with salt motion.
- *Conservation of energy*: Heat transfer in a multi-component system is considerably different than in a bulk medium. The composite medium can host several nonlinear phenomena, especially in the presence of multiphase fluids and fractures, because both salt and sediment rheology and reactivity depend strongly on temperature.
- *3-D computational platform*: To our knowledge, all previous salt simulators are limited to 2-D. Such studies have shown that salt instability can be triggered by buoyancy (if surrounding sediments are not lithified) or if the system is subjected to overall compression or extension. However, most salt bodies are subjected to a time-dependent multidimensional compression/extension history. Quite generally, nonlinear dynamic systems are known to have a strong dependence on spatial dimensionality (see, for example, Ortoleva, 1990, 1994a, in the context of geologic systems). Therefore, to have a better understanding of the motion of real salt bodies, a 3-D computational platform is required.
- *Coupling of sedimentation and salt motion*: In most studies, sedimentation and erosion are ignored. Our numeric technique accounts for nonuniform sedimentation or erosion associated with salt-motion-induced surface topology.
- *Evolving sediment and salt rheology*: Although salt rheology is fairly well approximated by existing laws, the rheology of the evolving sediment dictates the overall salt motion. Therefore, a model that can evolve sediment properties including poroelasticity and viscosity coefficients is

required for capturing the time dependence and spatial distribution of salt bodies.

Example Simulations

Several 2-D simulations were carried out to gain insight into the interaction among salt migration, sedimentation, fracturing, and fluid flow. Because the boundary conditions are chosen to be symmetric (no vertical shear stress and no horizontal displacement at both sides), only simulation of a half salt wave is sufficient to study the dynamics of such systems. The wavelength is taken as 10 km. Initially, the computational domain consists of a salt body underlying a shale layer. Then, alternating layers of shales and sandstones are added. The sedimentation distribution is modified so that the top surface remains horizontal during evolution, i.e., putative topographic variations are filled in by sedimentation. The initial relief in the salt geometry is 400 m. In 8 m.y., the salt relief reaches 3000 m, in the example shown in Figure 14.

To predict salt-tectonics-related petroleum pools, we must coevolve petroleum generation/expulsion/migration with salt and rock deformation. Figure 15
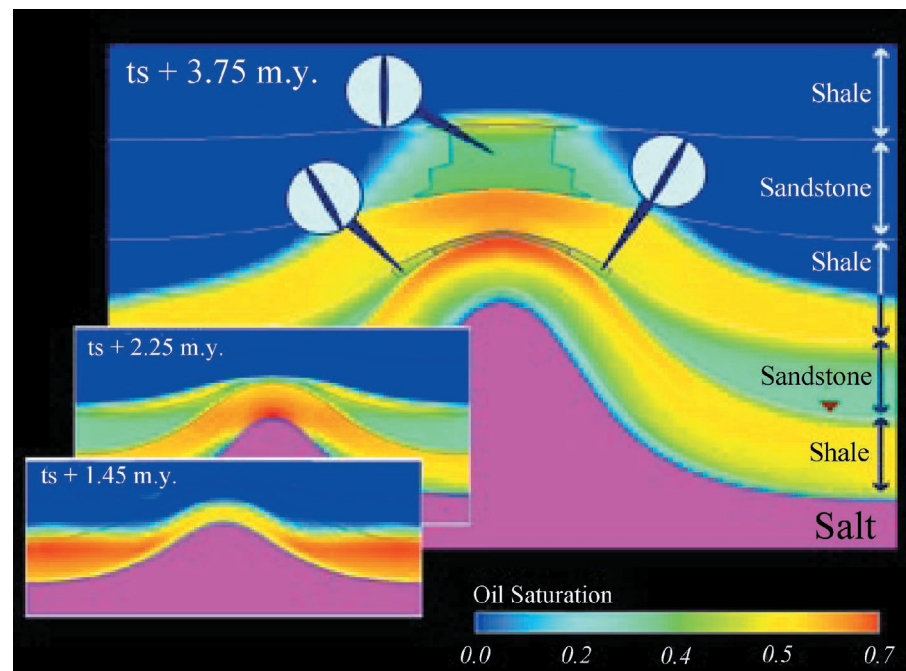

Figure 15. Simulated time sequence of oil saturation overlying a rising salt dome. Source rock overlying the dome was transiently over-pressured and fractured, facilitating upward oil migration within it and into the overlying layers. Orientations of long-lived fractures (residing in the sandstones) illustrate the relationship between the salt motion and fracture pattern. The location of oil depends strongly on the rate of salt motion and the coevolving mechanical and transport properties of the adjacent sediments.

shows an oil pool developed in association with salt diapirism. The oil was generated in a source rock overlying the salt, both of which were essentially flat in an early stage that preceded diapirism.

A similar situation, but for a subsalt source rock, is seen in Figure 16. Low permeability salt bodies form very efficient seals. In this simulation, the salt body is laterally discontinuous and resides above shale. The lower half of the shale is assumed to be source rock. As the salt body moves upwards, it drags the underlying shale layer. Because of the low permeability of salt, fluid can only flow around the salt body resulting in high overpressure at the center, which in return decreases the effective stress there.

Salt bodies are inherently 3-D. Even waves should be studied in 3-D, because they are likely to be vulnerable to lateral instabilities, forming diapirs along the wave. One expects that diapirism should be more rigorous in 3-D, because the rising body can draw on salt from a second lateral dimension (waves are fed from only one dimension). Figure 17 shows a quarter section of a salt diapir. The areal size of the computational domain was taken to be 5 × 5 km. Initially, the salt surface is a tilted plane, and there was a shale layer overlying the salt body. Because of the symmetry conditions at all four sides of the computational domain, the initial condition can also be viewed as a quarter section of a pyramid.
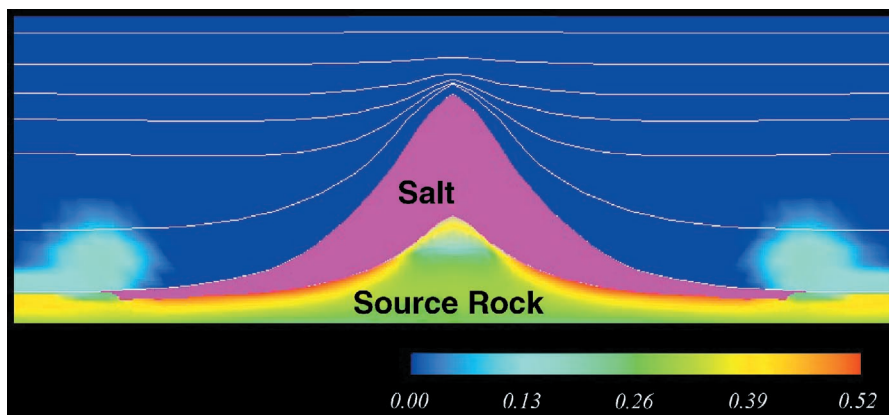

Figure 17. Simulated quarter section of a salt diapir showing the relationship to fracturing in the overlying sandstones after 3 m.y. of deformation. Extracted partial front cross section shows the fracture length.

CONCLUSIONS

The use of comprehensive, 3-D fully coupled basin models is absolutely essential because of two main reasons. First, simpler models (with fewer processes, lower dimensionality, and decoupled) miss many qualitative features of the dynamic petroleum systems. Second, because the real system has the complexity suggested in Figure 1, estimations appropriate for exploration and field development analysis are most reliably based on models with the required completeness.

The comprehensiveness, three-dimensionality, and fully coupled nature of the required basin model presents us with formidable computational challenges. We have addressed this challenge by parallelizing our Basin RTM simulator's modules. Furthermore, the development of hardware (notably gigaflop CPUs, multigigabyte RAM, and parallel architecture) is bringing fast, affordable computing to the wider E&P community.

Figure 16. Simulated time sequence of oil saturation overlying a rising salt dome, as in Figure 15, except for an initially finite size (lenticular) salt body and, in addition, the coevolution of subsalt petroleum. The oil saturation with curves indicating lithologic contacts is shown. The overpressure under the salt body and the stress regime on the underlying sediment have preserved porosity in the center region under the salt, and the compaction under the edge of the salt led to the formation of a seal. Thereby, a subsalt compartment is formed.
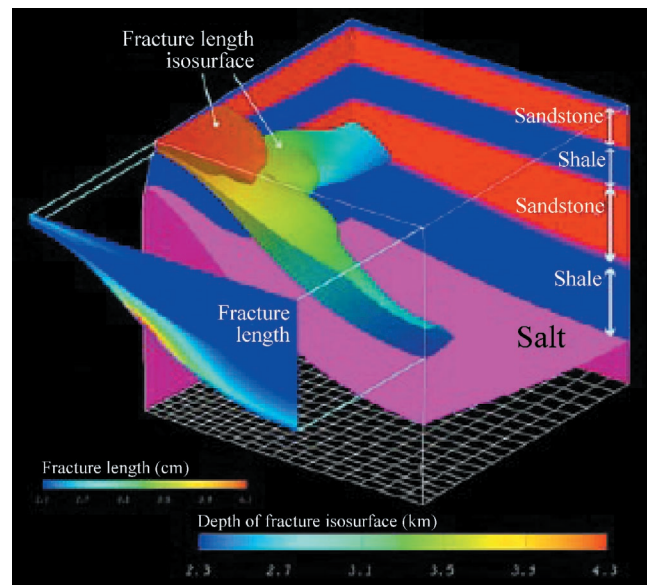
As we have completed our 3-D basin model, we have turned our attention to the development of more general and accurate physicochemical models. In particular, we are focusing on textural models and their implications for rheological laws and permeability and other flow parameters. We are developing a new multiphase flow phenomenology that accounts for the dynamic geometry of the various fluid phases as the dynamic petroleum system evolves.

In modeling such a complex system as a sedimentary basin, we encounter many limits to the accuracy of our estimations. The major limitations and the steps we are taking to control them are as follows.

- *Low spatial resolution*: Increasing the number of finite elements is becoming more feasible by improving hardware, computational efficiency, and parallelization.
- *Phenomenological laws*: The equations underlying Basin RTM evolution are continuously being improved, as is the calibration of the rate coefficients and other parameters.
- *Nonlinear dynamics/chaos*: The dynamic of a basin is highly nonlinear; such systems are well known to be sensitive to initial data and boundary effects. Through our extensive experience in the modeling of self-organizing and nonlinear oscillatory phenomena (Ortoleva, 1990, 1992, 1994a, 1994b; Renard and Ortoleva, personal communication, 2001), we have developed protocols for distinguishing between numeric noise and chaos or self-organized spatial structure.
- *Numeric inaccuracy*: This is well controlled using standard tests for convergence with respect to space or time steps and convergence criteria for iterative solution techniques.
- *Geologic input data*: We are limiting uncertainties caused by the interpretation of seismic, well log, surface, and other data through an automated integration of the data and Basin RTM using information theory.

Although there are many potential uncertainties in basin modeling, we believe that by use of modern mathematical and computational techniques and remote and other data analysis approaches, we can achieve the levels of accuracy and risk assessment for E&P applications.

Our results on fault dynamics, notably the earthquake cycle (Tuncay et al., 2001), and our extensive work on spontaneous pattern formation in geologic systems (see Ortoleva, 1994a) illustrate that the sedimentary basin is capable of spatial self-organization and periodic or chaotic temporal oscillation. The behaviors strongly suggest that a deeper understanding of sedimentary basin behavior is to come from the theory of nonlinear dynamic systems. We are using our Basin RTM simulator to delineate the types and conditions favoring these phenomena. Finally, we believe that these generic studies and our previous and ongoing simulation of the Piceance, west Texas, and east Texas basins illustrate the great practical potential of the application of comprehensive, 3-D coupled basin models to address key E&P challenges, estimating the location of reservoirs and their fracture, stress, fluid pressure, and fluid characteristics.

ACKNOWLEDGMENTS

APPENDIX A
INCREMENTAL STRESS RHEOLOGY

The strong coupling of deformation with the diagenetic, hydrologic, and thermal processes is captured in Basin RTM using an incremental stress rheology. The specific rheology used in Basin RTM integrates all the strain mechanisms believed to operate in a basin. It has the form (Tuncay et al., 2000a; Ortoleva, 1994a, 1998)

$$\dot{\underline{\underline{\varepsilon}}} = \dot{\underline{\underline{\varepsilon}}}^{\text{el}} + \dot{\underline{\underline{\varepsilon}}}^{\text{vp}} + \dot{\underline{\underline{\varepsilon}}}^{\text{ps}} + \dot{\underline{\underline{\varepsilon}}}^{\text{fr}} + \dot{\underline{\underline{\varepsilon}}}^{\text{go}}. \tag{A-1}$$

Here, $\dot{\underline{\underline{\varepsilon}}}$ is the net rate of strain, whereas the terms on the right give the specifics of five processes: poroelasticity (el), continuous viscoplastic (vp), pressure solution (ps), fracturing (fr), and gouge (go). Specific expressions for each term have been taken from the literature or newly developed for our RTM simulator (see Appendix C for the development of the rate-of-strain tensor caused by fracturing).

Let us make some of the coupling more explicit. The poroelasticity rate of strain $\dot{\underline{\underline{\varepsilon}}}^{\text{el}}$ may be expressed in terms of stress $\underline{\sigma}$, pressure p of the wetting fluid

phase, and rock texture Θ via

$$\underline{\dot{\varepsilon}}^{\text{el}} = \underline{\underline{C}}^{-1}(\Theta) \frac{D}{Dt}(\underline{\sigma} + \alpha(\Theta)p\underline{I}) \qquad (A\text{-}2)$$

for fourth-rank matrix of poroelastic coefficients $\underline{\underline{C}}$ and effective stress coefficient α. D/Dt represents a material time derivative measuring the rate of change of a tensor in time with respect to a local reference frame fixed to a translating, rotating material volume element. The texture Θ represents a set of variables characterizing the mineralogy, shape, size, orientation, and packing of the grains. In summary,

$$\underline{\dot{\varepsilon}}^{\text{el}} = \underline{\dot{\varepsilon}}^{\text{el}}(\Theta, p, \underline{\sigma}), \qquad (A\text{-}3)$$

illustrating the strong coupling among deformation, fluid properties, and texture.

A direct coupling of mechanics and chemistry arises through pressure solution. Grain dissolution at stressed grain-grain contacts induces compaction and thereby contributes to $\underline{\dot{\varepsilon}}$. The rate of this pressure solution contribution, $\underline{\dot{\varepsilon}}^{(\text{ps})}$, depends on the stress at grain-grain contacts and hence on the macrostress $\underline{\sigma}$, fluid pressure, and texture. However, $\underline{\dot{\varepsilon}}^{(\text{ps})}$ should also depend on the composition of the (assumed single-phase) pore fluid. The latter may be characterized by the set of concentrations $c = \{c_1, c_2, \cdots c_N\}$ for the N pore fluid species system; hence, $\underline{\dot{\varepsilon}}^{(\text{ps})}$ depends on $\underline{\sigma}$, Θ, p, and c.

Because the present theory is macroscopic, the variables describing fractures are considered to be part of the texture Θ. This assumes that the length scale on which the phenomena of interest vary is much greater than the fracture length or interfracture spacing. Otherwise, one must treat fractures individually, an approach that is not viable for basin-scale modeling. With our macrotextural description, one must allow for the potential influence of the fracture variables on rock mechanical and other properties (Appendix C).

One expects that $\underline{\dot{\varepsilon}}^{(j)}$, j = poroelasticity, viscosity, pressure solution, fracturing, gouge, etc., should depend generally on all the aforementioned variables ($\underline{\sigma}$, Θ, p, c) as well as absolute temperature T. With this,

$$\underline{\dot{\varepsilon}} = \sum_{j=1}^{N_{\text{d}}} \underline{\dot{\varepsilon}}^{(j)}(\Theta, \underline{\sigma}, p, c, T). \qquad (A\text{-}4)$$

The dependency of the $\underline{\dot{\varepsilon}}^{(j)}$ on the indicated state variables may be nonlocal in time. For example, in the case of poroelasticity, $\underline{\dot{\varepsilon}}^{(\text{pe})}$ depends on the time derivative of effective stress. Therefore, the $\underline{\dot{\varepsilon}}^{(j)}$ may be functions of their arguments that can, in principle, sample the state variables in some finite volume of space-time. The dependence of the strain rates on state clarifies the central role of incremental stress theory in integrating all the RTM basin processes into a unified model. It is the coupling allowed by this integration that underlies many key basin phenomena, from fault dynamics to episodic fluid flow, seal formation, and overpressure.

To complete the incremental stress formulation, explicit expressions for the rate functions $\underline{\dot{\varepsilon}}^{(j)}(\Theta, \underline{\sigma}, p, c, T)$ are required. For $\underline{\dot{\varepsilon}}^{(\text{ps})}$, for example, these can be obtained through geometric considerations of the texture variables and the rate of grain shortening from pressure solution (see Dewers and Ortoleva, 1994a; Ortoleva, 1994a, 1998).

The total rate of strain $\underline{\dot{\varepsilon}}$ is defined via

$$\dot{\varepsilon}_{ii'} = \frac{1}{2}\left(\frac{\partial u_i}{\partial x_{i'}} + \frac{\partial u_{i'}}{\partial x_i}\right). \qquad (A\text{-}5)$$

The six independent components of the symmetric second-rank tensor equation (A-3) must be supplemented with three additional equations so that the three deformation velocity components ($\underline{u} = u_1, u_2, u_3$) can be determined. The required condition arises from force balance

$$\sum_{i'=1}^{3} \frac{\partial \sigma_{ii'}}{\partial x_{i'}} + f_i = 0 \qquad (A\text{-}6)$$

for body force f_i which, for gravity, is given by

$$f_i = g\rho_{\text{m}}\delta_{i3}. \qquad (A\text{-}7)$$

Here, g is the gravitational acceleration, ρ_{m} is the mass density, and the 3-direction is upward.

The above formulation must be augmented with equations of texture dynamics and fluid mass and energy conservation (the latter to fix T). With this, our model provides a complete theory of basin dynamics where the equations are solved subject to the boundary conditions imposed by the overall tectonics and by the surficial fluids (i.e., ocean-bottom and atmospheric pressure).

Effects such as strain hardening or weakening are accounted for in the present model via the coupled dynamics of texture and stress. The differential

equations of texture evolution introduce the time delays (memory) that make our rheology capture hardening or softening. The latter properties are reflections of texture, i.e., hardness/weakness is a unique function of texture but not of stress. Thus, rock rheology depends on texture which, via the evolution equations of the latter, depends on the history of deformation.

In addition to the coupling of deformation to other phenomena through the incremental stress formulation, there are numerous indirect couplings. For example, rock properties such as permeability, multiphase flow parameters, reactive grain surface area, and thermal conductivity depend strongly on texture. Because stress and deformation affect texture, a complex network of coupling relations is thereby expressed. For further discussion of the consequence of this network, see Ortoleva (1994a, 1994b, 1998), Tuncay et al. (2000a, b), Ozkan et al. (1998), and Dewers and Ortoleva (1994b).

APPENDIX B
ROCK COMPETENCY

Sedimentary rock deformation is a multiple time- and length-scale phenomenon. Rocks fail abruptly but heal slowly on geologic timescales (Fredrich and Evans, 1992; Logan and Teufel, 1986). Brittle rocks have two sources of memory. They store elastic energy and, once failed, have broken grain-grain contacts and gouge that persist over long periods of time. Viscous deformation or failure erases the former, whereas chemical healing processes diminish or erase the latter. When sheared across a large-scale zone, they can fail within a meter-scale fault zone. Furthermore, the fault dynamic typically takes the form of a series of short timescale events with long interevent healing periods to form the earthquake cycle. The challenge is to develop a rheological model of this deformation behavior that captures this multiple-scale character autonomously— i.e., from an initially uniform, unfailed system to a faulted one experiencing intermittent failure-healing cyclicity and complex spatial structure.

The rate- and state-dependent friction models introduce several state variables that are governed by ordinary differential equations (Dieterich, 1979; Ruina, 1983; Rice and Gu, 1983; Rice and Ruina, 1983; Tse and Rice, 1986). The physical interpretations of these state variables are commonly ambiguous. A more general approach is the use of texture variables such as grain-size distribution, porosity, and packing as the state variables of the system. The key to this approach is that the memory of rocks is to be captured by a sufficiently rich textural model and that the texture, must be coevolved with rock stress and deformation to yield a self-consistent model of strain hardening/weakening, fault narrowing, and earthquake cyclicity. In the present study, these multiple-scale and autonomous-fault behaviors are shown to follow naturally from the feedback between stress and rock texture, as suggested in Figure 1. Rock deformation is thereby autonomous— stress changes texture, texture changes rock rheology, and rock rheology affects stress. This feedback is shown here to be more self-consistent and fundamental than concepts such as strain hardening/weakening or velocity-dependent viscosity.

We suggest that rigorous models of rock behavior should be of the Markov type— i.e., the rate of change of rock state should depend only on the instantaneous rock state and not on prior history. Stress and strain are related through rock rheology to rock texture Θ (grain size, shape, packing, and mineralogy). Pressure solution and grain breakage imply that the rate of change of Θ depends on stress, denoted σ. If Θ satisfies the differential equation (1), then in principle, $\Theta(t)$ is a function of σ, i.e., dependent on $\sigma(t')$ for all $t' < t$, i.e., on the stress history: $\Theta = \Theta[\sigma]$. Because rheology depends on Θ, we see that $\Theta[\sigma]$ reflects the entire prior stress history and not just the instantaneous value of σ. Clearly, however, this "memory" in a theory wherein Θ is not coevolved with σ is an artifact of the incompleteness of a rock deformation model that attempts to avoid coevolving Θ with stress. Although there are many stress-strain histories that could lead to the instantaneous state of a rock, only the latter is key to estimating its failure and other behavior.

Let Γ, rock competency, measure the fraction of grain surface that is attached to other grains. Thus, Γ is in the range $0 \leq \Gamma \leq 1$. Large Γ implies competency, whereas in a low-Γ rock, there are few intact grain-grain contacts. Thus, rheological quantities such as rock strength or viscosity are strongly dependent on Γ.

Schematically, our model is as follows. The equation of motion of Γ is taken in the form

$$\frac{\mathrm{D}\Gamma}{\mathrm{D}t} = R(\Gamma, F) \qquad \text{(B-1)}$$

where F is a failure function that depends on macroscopic stress, fluid pressure, rock texture, mineralogy, and temperature. In three dimensions, the failure function is assumed to take the form

$$F = aJ_1 + \sqrt{J_2} - b \qquad \text{(B-2)}$$

where J_1 is the first invariant of the effective stress tensor and J_2 is the second invariant of the deviatoric effective stress tensor. The coefficients a and b can be expressed in terms of angle of internal friction φ and cohesion C, determined from conventional triaxial compression experiments (Desai and Siriwardane, 1984)

$$a = \frac{2\sin\varphi}{\sqrt{3}(3 - \sin\varphi)} \qquad \text{(B-3)}$$

$$b = \frac{6C\cos\varphi}{\sqrt{3}(3 - \sin\varphi)}. \qquad \text{(B-4)}$$

Here, we assume that cohesion depends on rock competency. For an intact rock ($\Gamma = 1$), b is large. As the rock competency is lost, the cohesionlike term b vanishes. Therefore, b is a strong function of Γ, taken here to be $b = b^*\Gamma^n$, where b^* refers to the value when $\Gamma = 1$ and n is a phenomenological exponent.

If the dynamics of Γ is relatively fast, its evolution is closely related to the shape of the curve $R(\Gamma, F) = 0$ (see Chapters 2 and 3 of Ortoleva, 1992, for further discussion). The Γ dynamics is, in a sense, a cooperative phenomenon, i.e., a decrease in competence fosters more rapid Γ decline. The qualitative picture of Figure B-1 captures this. A schematic evolution path in the F, Γ plane is shown.

Through this model, failure is rapid, whereas healing can be a much slower process. This follows if R is relatively small where Γ is small and F is less than a healing value F_h. This type of effect gives geologic materials the memory they have of zones of earlier faulting. Here, $R(\Gamma, F)$ is taken in the form

$$R(\Gamma, F) = k(\Gamma, F)$$

$$\times \left(-F + d_3\left(\frac{1}{2} - \Gamma\right) + \frac{d_2}{\Gamma} + \frac{d_1}{1 - \Gamma} + d_4 \right)\Gamma(1 - \Gamma) \qquad \text{(B-5)}$$

where d_1, d_2, d_3, and d_4 are material constants. The function k is chosen such that if Γ is small and $F < F_h$, k is small, ensuring that healing is slow. Finally, F_h

can be determined in terms of d_1, d_2, d_3, and d_4. Conceptually, these parameters depend on mineralogy, grain size, shape, and packing.

We now show that the feedback associated with the coupling of shear stress (via incremental stress rheology) and rock competency naturally support autonomous oscillation. Consider a simple shear system with the total rate of strain given by the sum of poroelastic and nonlinear viscous contributions. The following ordinary differential equation for the shear stress follows from the incremental stress rheology of Appendix A:

$$\frac{D\tau}{Dt} = \frac{G_f}{\mu(\Gamma)}(2\dot{\varepsilon}\mu(\Gamma) - \tau) \qquad \text{(B-6)}$$

where τ, $\dot{\varepsilon}$, G_f, and μ are the shear stress, total rate of shear strain, elastic shear modulus, and shear viscosity, respectively. Shear viscosity is taken to be an increasing function of rock competency $\mu = \mu^*\Gamma^m$. The exponent m is taken as 8 to capture the large change in the order of magnitude of shear viscosity between intact and failed rock. The rate of shear strain is either taken to be a specified function of time or determined by the energy dissipation condition

$$\tau\dot{\varepsilon} = \dot{E} \qquad \text{(B-7)}$$

where $\dot{E}$ is the rate of energy input.
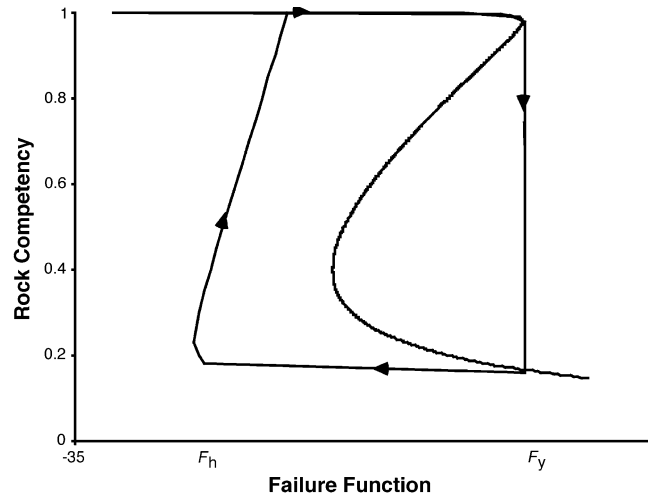

Figure B-1. Schematic competence (Γ) and failure function (F) plane illustrating the cooperative aspects of rock failure. When Γ is near unity, the rock is competent, but when F exceeds F_{yield}, it is compromised. However, for $F < F_h$, competence is regained through chemical healing processes.

Equations (B-1) and (B-6) form a strongly coupled set of non-linear ordinary differential equations for the shear stress and rock competency that were integrated numerically by the fourth-order Runga-Kutta technique with adaptive time stepping. Setting the RHS (equation [B-6]) to zero yields for constant $\dot{E}$ and the Drucker-Prager failure function (equation [B-2]),

$$\Gamma = \left(\frac{(F+c)^2}{2\mu^*\dot{E}}\right)^{1/m}. \qquad (B-8)$$

Figure B-2 illustrates the null curves for different values of $\dot{E}$. For small $\dot{E}$, the stress null curve (equation [B-7]) intersects the S-shaped null curve $R = 0$ on the upper stable branch near $\Gamma = 1$ (competent rock), i.e., the competent rock viscosity μ^* is sufficiently low so that the rate of energy input is equal to the rate of viscous energy dissipation (ductile flow). For very large $\dot{E}$, rock fails but the null curves intersect at the lower stable branch, i.e., the rock remains failed because of the very low shear viscosity needed to dissipate the required energy (aseismic faults). For intermediate values of $\dot{E}$, the null curves intersect at the unstable branch of $R = 0$. In this case, for a constant $\dot{E}$, rock fails and heals cyclically (seismic faults). It is also possible that the null curves intersect at three distinct points. In this case, depending on the initial conditions of shear stress and rock competency, rock will either never fail or never heal. If a point (F, Γ) is above the null curve given by equation (B-8), the shear stress increases; otherwise, it decreases. Similarly, if a point (F, Γ) is to the right of the null curve $R = 0$, the rock competency decreases. These four cases suggest a classification of fault dynamics— intact stable sliding, failed stable sliding, multiple state, and oscillatory sliding.

In the previous discussion, it is assumed that the shear viscosity is a function of rock competency only. In fact, shear viscosity depends strongly on porosity and grain-size distribution, i.e., $\mu^* = \mu^*(\Theta)$. Because of grain-size distribution, temperature-dependent intrinsic viscosity of minerals, and porosity change, the null curve given by equation (B-8) can be viewed as an instantaneous func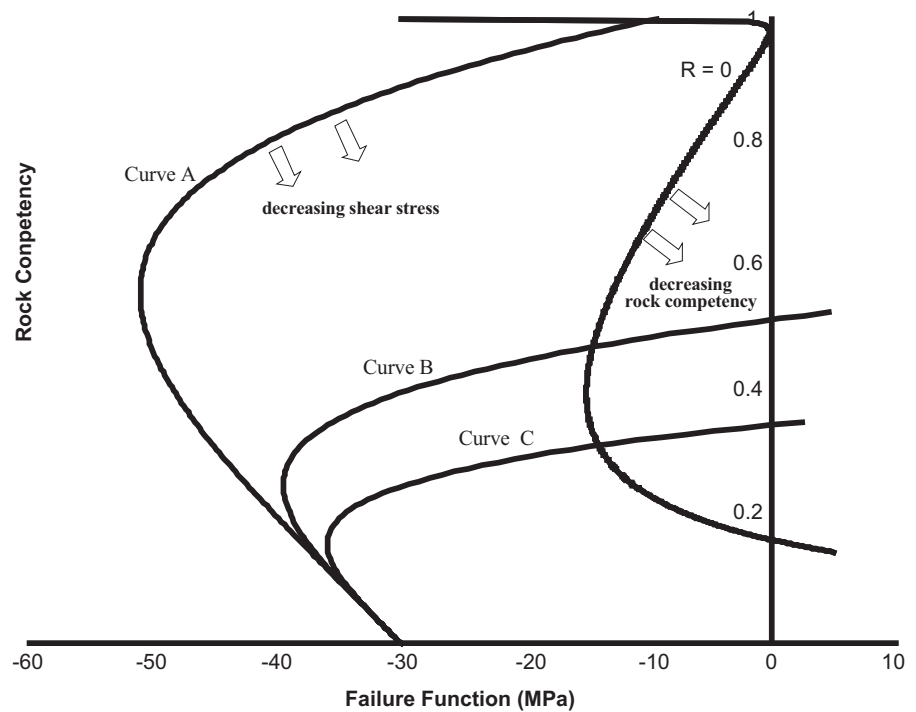tion of rock texture. For example, as the grains get smaller because of gouge, the shear viscosity decreases and the stress null curve tends to intersect the S-shaped curve ($R = 0$) at lower or higher Γ values, depending on the S-shaped curve. Similarly, particle-size increase because of diagenesis can significantly change the behavior. Thus, gouge and diagenesis can determine which of the modes of fault behavior noted above are realized for a given fault system.

Failure is a fast process, whereas healing is a slow one. Therefore, the coefficient k in equation (B-5) is very large when the (F, Γ) point is to the right of the S-shaped curve. However, for low shear viscosities (low Γ values), it is anticipated that the solution will follow equation (B-8) rather than the S-shaped curve ($R = 0$), because k is small in this region.

Equations (B-1) and (B-6) are generalized to include the fluid pressure, porosity, and other components of the stress tensor (Tuncay et al., 2001).

Figure B-2. The null curves for equations (B-1) and (B-6) for different values of $\dot{E}$.

APPENDIX C
FRACTURE NETWORK
STATISTICAL DYNAMICS MODEL

We have developed a model of the probability for fracture length, aperture, and orientation (Tuncay et al., 2000b). The model estimates the evolution of this probability in response to the changing stress,

fluid pressure, and rock properties as the basin changes. The fracture probability is used to compute the permeability tensor. The latter affects the direction of petroleum migration, information that is key to finding new resources. It is central to planning infill drilling spacing and likely directions for field extension. It is key to the design of horizontal wells and the optimum rate of production in stress-sensitive reservoirs. Finally, the estimated distribution of fracture network statistics across a field is a necessary input to reservoir simulators used to optimize production.

The dynamics of the fracture network in our model is based on a statistical representation. For example, consider a set of fractures of length L with normal $\underline{n}$ for a 3-D spectrum of normal orientations. Then, the rate of change for L in the rock-fixed frame takes the form

$$\frac{\mathrm{d}L}{\mathrm{d}t} = R(L, a, p, \Theta, \underline{\underline{\sigma}}) \qquad \text{(C-1)}$$

where the fracture extension rate R depends on the normal stress σ, the wetting phase fluid pressure p, and the texture Θ of the surrounding rock, and a is the aperture of the n-fracture. A similar equation for the fracture aperture is developed (see Tuncay et al., 2000b, for further details).

Let η' be the number density of sites where fractures may nucleate. By definition of the undeformed rock, $\eta' = \eta$ (η being the original depositional value of η'), but η' can differ from η because of changes in rock texture from diagenesis or mechanical processes. In the simplest case where fracture nucleation sites are not created or destroyed, η' obeys the conservation equation $\partial\eta'/\partial t + \underline{\nabla} \cdot (\eta'\underline{u}) = 0$. In a macrovolume element of volume V, there are $V\eta'$ fractures, and hence a fracture void space $V\eta'\pi L^2 a$ where a and L are the aperture and length (radius) of the assumed penny-shaped fractures, respectively. To compute the dilatation, we focus on a fixed volume V_m of solids and follow its change in a time δt. The volume of the unfractured rock V_{unfr} is related to V_m and the porosity ϕ_m of the unfractured rock via $V_{unfr} = V_m + \phi_m V_{unfr}$. Hence, $V_{unfr} = V_m/(1 - \phi_m)$. The total volume V of the sample of rock containing V_m is then

$$V = (1 - \phi_m)^{-1} V_m + V\Delta \qquad \text{(C-2)}$$

where $\Delta = \eta'\pi L^2 a$. With this, the volume of rock $V(t)$ at time t for fixed volume of solids V_m (considered

incompressible and not to expand thermally or react) is given by

$$V(t) = V_m(1 - \phi_m)^{-1}(1 - \Delta). \qquad \text{(C-3)}$$

Noting that

$$tr\underline{\underline{\dot{\varepsilon}}}^{(fr)} = \lim_{\delta t \to 0} \frac{V(t + \delta t) - V(t)}{V(t)\,\delta t} \qquad \text{(C-4)}$$

one obtains

$$tr\underline{\underline{\dot{\varepsilon}}}^{(fr)} = [1 - \Delta]^{-1}\frac{\mathrm{D}\Delta}{\mathrm{D}t} \qquad \text{(C-5)}$$

where $\mathrm{D}/\mathrm{D}t$ is the material derivative, i.e., the derivative in the reference frame fixed to the solids.

The tensor character of the fracture-mediated deformation is related to the directions of each fracture through its normal n to the fracture plane. Consider the expression

$$\dot{\varepsilon}_{kl}^{(fr)} = [1 - \Delta]^{-1}\frac{\mathrm{D}}{\mathrm{D}t}(\Delta n_k n_l). \qquad \text{(C-6)}$$

Here, $\mathrm{D}/\mathrm{D}t$ represents a material time derivative; however, now it also must account for the rotation of the fracture normals as they change direction with flexure, shearing, or other deformation. Note that the trace of this expression agrees with the earlier result for the dilatation. Finally, this expression agrees with simple cases wherein all fractures are parallel.

In our model, a finite (but representative) number of fracture orientations is accounted for. We use the fracture kinetics formulation of Ortoleva (1994a) and Sonnenthal and Ortoleva (1994). However, here we replace the least compressive stress in the formulation by the stress component normal to each fracture plane. This allows calculation of fracture length and aperture for each fracture orientation. For example, if we assume that only vertical fractures can occur as for a 1-D problem, because the stress component normal to any vertical plane is the same because of the symmetry, an isotropic fracture network develops. In 3-D problems, our proposed algorithm has the power to estimate a complex fracture network with preferential orientations dictated by the structure of the stress tensor.

Because the fracture network is well defined, the anisotropic fracture permeability can be calculated

approximately. The anisotropic fracture permeability of a fracture network consisting of a single fracture orientation is given by

$$K_{ij}^{\text{fr}} = \lambda(\delta_{ij} - n_i n_j) \qquad \text{(C-7)}$$

where n is the unit normal to the fracture plane and $\underline{\underline{K}}^{\text{fr}}$ is the fracture permeability. The parameter λ can be approximated by

$$\lambda = \beta \phi_{\text{fr}} \frac{a^2}{12}. \qquad \text{(C-8)}$$

Here, β is a factor accounting for the connectivity of fractures. For large fracture lengths and dense networks, β approaches unity, whereas for small fracture lengths and low fracture densities, it vanishes (Oda, 1986). Oda (1985, 1986) proposed that this coefficient should be a function of a dimensionless second-order tensor of fracture geometry. He called this tensor the ''fabric tensor'' (Oda, 1982). A discussion of this factor can be found in the papers of Oda (1985, 1986). In this study, β is taken as unity. We assume that the total fracture permeability is obtained by summation of fracture permeabilities for all orientations and statistical classes multiplied by the fracture porosity, which has been proposed previously by Chen et al. (1999). It is assumed that fluid flow is slow and the disturbance at fracture intersections is negligible. Summation is inadequate when the fracture density is lower than the percolation threshold (Berkowitz, 1995; Odling, 1992; Bour and Davy, 1998). The surface roughness of fractures causes another limitation. In this study, fracture aperture is assumed to be constant in a particular fracture. The spatial distribution of fracture aperture alters the fracture permeability. Waite et al. (1998) measured water flow through a sinusoidal fracture to compare sinusoidal flow with parallel plate flow. Their experimental and numeric results showed that a sinusoidal fracture has a significantly lower permeability, and for the sinusoidal geometry, the effective aperture is very close to the minimum value of the normal aperture. Thomson and Brown (1991) showed that the directional nonuniformities in the fracture surface are more important than the degree of surface roughness. Therefore, equation (C-7) should be viewed as a simple fracture permeability tensor to approximate dense fracture networks with relatively smooth fracture surface. Note that the fracture permeability tensor is obtained by postprocessing the fracture network characteristics.

We refer to Tuncay et al. (2000b) for further details.

REFERENCES CITED

Abriola, L. M., and K. Rathfelder, 1993, Mass balance errors in modeling two-phase immiscible flows: Causes and remedies: Advances in Porous Media, v. 16, p. 223–239.

Atkinson, B. K., 1984, Subcritical crack growth in geological materials: Journal of Geophysical Research, v. 89, p. 4077–4114.

Aubertin, M., S. Servant, and D. E. Gill, 1994, Experimental identification of kinematic and isotropic hardening in rocksalt, in P. P. Nelson and S. E. Laubach, eds., Rock mechanics: Rotterdam, Balkema, p. 723–730.

Bathe, K. J., 1996, Finite element procedures: Englewood Cliffs, New Jersey, Prentice Hall, 1037 p.

Bathe, K. J., E. Ramm, and E. L. Wilson, 1975, Finite element formulations for large deformation dynamic analysis: International Journal for Numerical Methods in Engineering, v. 9, p. 353–386.

Berkowitz, B., 1995, Analysis of fracture network connectivity using percolation theory: Mathematical Geology, v. 27, p. 467–483.

Berryman, J. G., 1980, Long-wavelength propagation in composite elastic media, I: Spherical inclusions: Journal of the Acoustical Society of America, v. 68, p. 1809–1819.

Berryman, J. G., 1986, Effective medium approximation for elastic constants of porous solids with microscopic heterogeneity: Journal of Applied Physics, v. 59, p. 1136–1140.

Biot, M. A., 1966, Three dimensional gravity instability derived from two-dimensional solutions: Geophysics, v. 31, p. 153–166.

Biot, M. A., and H. Ode, 1965, Theory of gravity instability with variable overburden and compaction: Geophysics, v. 30, p. 213–227.

Bour, O., and P. Davy, 1998, On the connectivity of three-dimensional fault networks: Water Resource Research, v. 34, p. 2611–2622.

Brantley, S., B. Evans, S. H. Hickman, and D. A. Crear, 1990, Healing of microcracks in quartz: Implications for fluid flow: Geology, v. 18, p. 136–139.

Budiansky, B., and R. J. O'Connell, 1976, Elastic moduli of a cracked solid: International Journal of Solids and Structures, v. 12, p. 81–97.

Carter, N. L., S. T. Horseman, J. E. Russell, and J. Haydin, 1993, Rheology of rocksalt: Journal of Structural Geology, v. 15, p. 1257–1271.

Chen, M., M. Bai, and J.-C. Roegiers, 1999, Permeability tensors of anisotropic fracture networks: Mathematical Geology, v. 31, p. 355–373.

Cobbold, P. R., ed., 1993, New insights into salt tectonics: Collection of invited papers reflecting the recent developments in the field of salt tectonics: Tectonophysics, v. 228, p. 141–445.

Currie, J. B., and S. O. Nwachukwu, 1974, Evidence on incipient fracture porosity in reservoir rocks at depth: Bulletin of Canadian Petroleum Geology, v. 22, p. 42–58.

Daudre, B., and S. Cloetingh, 1994, Numerical modeling of salt diapirism: Influence of the tectonic regime: Tectonophysics, v. 240, p. 59–79.

De Las Cuevas, C., 1997, Pore structure characterization in rock salt: Engineering Geology, v. 47, p. 17–30.

Desai, C. S., and H. J. Siriwardane, 1984, Constitutive laws for engineering materials: Englewoods Cliffs, New Jersey, Prentice Hall, 487 p.

Dewers, T., and P. Ortoleva, 1994a, Formation of stylolites, marl/limestone alternations, and dissolution (clay) seams by unstable chemical compaction of argillaceous carbonates, in K. H. Wolf and G. V. Chilingarian, eds., Diagenesis, IV: Developments in sedimentology 51: New York, Elsevier, p. 155–216.

Dewers, T., and P. Ortoleva, 1994b, Nonlinear dynamical aspects of deep basin hydrology: Fluid compartment formation and episodic fluid release: American Journal of Science, v. 294, p. 713–755.

Dieterich, J. H., 1979, Modeling of rock friction, 1: Experimental results and constitutive equations: Journal of Geophysical Research, v. 84, p. 2161–2168.

Dutton, R., 1974, The propagation of cracks by diffusion, in R. C. Bradt, D. P. H. Hasselman, and F. F. Lange, eds., Fracture mechanics of ceramics, v. 2: Symposium on the fracture mechanics of ceramics: New York, Plenum Press, p. 649–657.

Engelder, T., 1987, Joints and shear fractures in rock, in B. K. Atkinson, ed., Fracture mechanics of rocks: Orlando, Academic Press, p. 27–69.

Engelder, T., and P. Geiser, 1980, On the use of regional joint sets as trajectories of paleostress fields during the development of the Appalachian Plateau, New York: Journal of Geophysical Research, v. 85, p. 6319–6341.

Fischer, M. P., M. R. Gross, T. Engelder, and R. J. Greenfield, 1995, Finite element analysis of the stress distribution around a pressurized crack in layered elastic medium—Implications for the spacing of fluid-driven joints in bedded sedimentary rock: Tectonophysics, v. 247, p. 49–64.

Fredrich, J. T., and B. Evans, 1992, Strength recovery along simulated faults by solution transfer processes, in J. R. Tillerson and W. R. Warersik, eds., 33rd U.S. Rock Mechanics Symposium: Rotterdam, Balkema, p. 121–130.

Friedman, M., 1976, Fracture in rock: Reviews of Geophysics and Space Physics, v. 13, p. 352–358, 383–389.

Gross, M. R., 1993, The origin and spacing of cross joints—Examples from the Monterey formation, Santa Barbara coastline, California: Journal of Structural Geology, v. 15, p. 737–751.

Haase, S., J. Chadam, D. Feinn, and P. Ortoleva, 1980, Oscillatory zoning in plagioclase feldspar: Science, v. 209, p. 272–274.

Hancock, P. L., A. Al Kadhi, and J. L. Walper, 1984, Regional joint sets in the Arabian platform as indicators of intraplate processes: Tectonics, v. 3, p. 27–43.

Harris, J. F., G. L. Taylor, and J. L. Walper, 1960, Relation of deformational fractures in sedimentary rocks to regional and local structure: AAPG Bulletin, v. 44, p. 1853–1873.

Huyakorn, P. S., S. Panday, and Y. S. Wu, 1994, A three dimensional multiphase flow model for assessing NAPL contamination in porous and fractured media, I: Formulation: Journal of Contaminant Hydrology, v. 16, p. 109–130.

Jackson, M. P. A., and C. J. Talbot, 1986, External shapes, strain rates, and dynamics of salt structures: Geological Society of America Bulletin, v. 97, p. 305–323.

Koudina, N., R. G. Garcia, J.-F. Thovert, and P. M. Adler, 1998, Permeability of three-dimensional fracture networks: Physical Review E, v. 57, p. 4466–4479.

Kulander, B. R., C. C. Barton, and S. L. Dean, 1979, The application of fractography to core and outcrop fracture investigations, Report METC/SP-79/3: U.S. Department of Energy, Morgantown Energy Technology Center, 174 p.

Larson, K. W., D. W. Waples, H. Fu, and K. Kodama, 1993, Predicting tectonic fractures and fluid flow through fractures in basin modeling, in A. G. Dore, ed., Basin modeling: Advances and applications, NPF Special Publications 3: Amsterdam, Elsevier, Norwegian Petroleum Society, p. 373–383.

Logan, J. M., and L. W. Teufel, 1986, The effect of normal stress on the real area of contact during frictional sliding of rocks: Pure and Applied Geophysics, v. 124, p. 471–486.

Long, J. C. S., and D. M. Billaux, 1987, From field theory to fracture network modeling: An example incorporating spatial structure: Water Resources Research, v. 23, p. 1201–1216.

Lorenz, J. C., L. W. Teufel, and N. R. Warpinski, 1991, Regional fractures I: A mechanism for the formation of regional fractures at depth in flat-lying reservoirs: AAPG Bulletin, v. 75, p. 1714–1737.

Luo, X., and G. Vasseur, 1996, Geopressuring mechanism of organic matter cracking: Numerical modeling: AAPG Bulletin, v. 80, p. 856–873.

Luo, X., G. Vasseur, A. Pouya, V. Lamoureux-Var, and A. Poliakov, 1998, Elastoplastic deformation of porous medium applied to the modeling of compaction at basin scale: Marine and Petroleum Geology, v. 15, p. 145–162.

Mallory, W. W., 1977, Oil and gas from fractured shale reservoirs in Colorado and northwest New Mexico: Rocky Mountain Association of Geologists Special Publication 1, 38 p.

Maubeuge, F., and I. Lerche, 1993, A north Indonesian basin: Geo, thermal and hydrocarbon generation histories: Marine and Petroleum Geology, v. 10, p. 231–245.

Maubeuge, F., and I. Lerche, 1994, Geopressure evolution

and hydrocarbon generation in a north Indonesian basin: Two-dimensional quantitative modeling: Marine and Petroleum Geology, v. 104, p. 104–115.

Mazariegos, R., M. J. Andrews, and J. E. Russell, 1996, Modeling the evolution of salt structures using nonlinear rocksalt flow laws: Tectonophysics, v. 256, p. 129–143.

Munson, D. E., and P. R. Dawson, 1984, Salt constitutive modeling using mechanism maps, in H. R. Hardy Jr. and M. L. Langer, eds., Proceedings of the First International Conference on the Mechanical Behavior of Salt: Clausthal, Germany, Trans Tech Publications, p. 717–737.

Nickelsen, R. P., and V. N. D. Hough, 1967, Jointing in the Appalachian Plateau of Pennsylvania: Geological Society of America Bulletin, v. 78, p. 609–630.

Nicolis, G., 1995, Introduction to nonlinear science: Cambridge University Press, 270 p.

Nicolis, C., and G. Nicolis, eds., 1987, Irreversible phenomena and dynamical systems analysis in geosciences: Dordrecht, Netherlands, D. Reidel Publishing Co., 608 p.

Nicolis, G., and I. Prigogine, 1977, Self-organization in nonequilibrium systems: New York, John Wiley & Sons, 512 p.

O'Connell, R. J., and B. Budiansky, 1977, Viscoelastic properties of fluid-saturated cracked solids: Journal of Geophysical Research, v. 82, p. 5719–5735.

Oda, M., 1982, Fabric tensor for discontinuous geological materials: Soils and Foundations, v. 22, p. 96–108.

Oda, M., 1985, Permeability tensor for discontinuous rock masses: Geotechnique, v. 35, p. 483–495.

Oda, M., 1986, An equivalent continuum model for coupled stress and fluid flow analysis in jointed rock masses: Water Resources Research, v. 22, p. 1845–1856.

Odling, N. E., 1992, Network properties of a two-dimensional natural fracture pattern: Pure and Applied Geophysics, v. 138, p. 95–114.

Ortoleva, P., ed., 1990, Self-organization in geological systems: Earth Science Reviews, v. 29, no. 1–4, 417 p.

Ortoleva, P., 1992, Nonlinear chemical waves: New York, John Wiley & Sons, 302 p.

Ortoleva, P., 1994a, Geochemical self-organization: New York, Oxford University Press, 411 p.

Ortoleva, P., ed., 1994b, Basin compartments and seals: AAPG Memoir 61, 477 p.

Ortoleva, P., 1998, Basin compartment fundamentals, Topical Report (Project No. GRI-97/0097): Chicago, Gas Research Institute, 452 p.

Ortoleva, P., E. Merino, J. Chadam, and C. H. Moore, 1987a, Geochemical self-organization, I: Reaction-transport feedback mechanisms and modeling approach: American Journal of Science, v. 287, p. 979–1007.

Ortoleva, P., E. Merino, C. H. Moore, and J. Chadam, 1987b, Geochemical self-organization, II: The reactive-infiltration instability: American Journal of Science, v. 287, p. 1008–1040.

Ortoleva, P., J. M. Maxwell, D. Payne, W. Sibo, and J. Comer, 1997, Naturally fractured reservoirs and compartments: A predictive basin modeling approach, in T. E. Hoak, A. L. Klawitter, and P. K. Blomquist, eds., Fractured reservoirs: Characterization and modeling, Rocky Mountain Association of Geologists Guidebook: Denver, Rocky Mountain Association of Geologists, p. 67–102.

Ozkan, G., and P. Ortoleva, 2000, Evolution of gouge grain size distribution: A Markov model: Pure and Applied Geophysics, v. 157, p. 10510–10525.

Ozkan, G., K. Tuncay, and P. Ortoleva, 1998, Process-based fault seal/conduit prediction, in 1998 AAPG annual convention abstracts (CD-ROM format), Salt Lake City, Utah, May 17–28, 1998.

Payne, D. F., K. Tuncay, A. Park, J. Comer, and P. Ortoleva, 2000, A reaction-transport-mechanical approach to modelling the interrelationships between gas generation, overpressuring, and fracturing—Implications for the Upper Cretaceous natural gas reservoirs of the Piceance Basin, Colorado: AAPG Bulletin, v. 84, p. 545–565.

Pollard, D. D., and A. Aydin, 1988, Progress in understanding jointing over the past century: Geological Society of America Bulletin, v. 100, p. 1181–1204.

Rice, J. R., 1975, Continuum mechanics and thermodynamics of plasticity in relation to microscale deformation mechanisms, in A. S. Argon, ed., Constitutive equations in plasticity: Cambridge, Massachusetts, MIT Press, p. 23–79.

Rice, J. R., 1992, Fault stress states, pore pressure distributions, and the weakness of the San Andreas Fault, in B. Evans and T.-F. Wong, eds., Fault mechanics and transport properties in rocks: London, Academic Press, p. 475–503.

Rice, J. R., and J. C. Gu, 1983, Earthquake aftereffects and triggered seismic phenomena: Pure and Applied Geophysics, v. 121, p. 187–219.

Rice, J. R., and A. Ruina, 1983, Stability of steady frictional slipping: Journal of Applied Mechanics, v. 50, p. 343–349.

Roberts, S. J., and J. A. Nunn, 1995, Episodic fluid expulsion from geopressured sediments: Marine and Petroleum Geology, v. 12, p. 195–204.

Ruina, A., 1983, Slip instability and state variable friction laws: Journal of Geophysical Research, v. 88, p. 10359–10370.

Schneider, F., J. L. Potdevin, S. Wolf, and I. Faille, 1996, Mechanical and chemical compaction model for sedimentary basin simulators: Tectonophysics, v. 263, p. 307–317.

Schultz-Ela, D. D., M. P. A. Jackson, and B. C. Vendeville, 1994, Mechanics of active diapirism, Report of Investigation No. 224: Bureau of Economic Geology, Austin, Texas, 56 p.

Segall, P., 1984, Rate-dependent extensional deformation resulting from crack growth in rock: Journal of Geophysical Research, v. 89, p. 4185–4195.

Segall, P., and D. D. Pollard, 1983, Joint formation in granitic rock of the Sierra Nevada: Geological Society of America, v. 94, p. 563–575.

Seni, S. J., and M. P. A. Jackson, 1984, Sedimentary record of Cretaceous and Tertiary salt movement, East Texas Basin, Report of Investigations No. 139: Bureau of Economic Geology, Austin, Texas, 89 p.

Sonnenthal, E., and P. J. Ortoleva, 1994, Numerical simulations of overpressured compartments in sedimentary basins, *in* P. J. Ortoleva, ed., Basin compartments and seals, AAPG Memoir 61, p. 403–416.

Spencer, C. W., 1987, Hydrocarbon generation as a mechanism for overpressuring in Rocky Mountain region: AAPG Bulletin, v. 71, p. 368–388.

Thomson, M. E., and S. R. Brown, 1991, The effect of anisotropic surface roughness on flow and transport in fractures: Journal of Geophysical Research, v. 96, p. 21923–21932.

Tse, S. T., and J. R. Rice, 1986, Crustal earthquake instability in relation to the depth variation of frictional slip properties: Journal of Geophysical Research, v. 91, p. 9452–9472.

Tuncay, K., and P. Ortoleva, 2001, Salt tectonics as a self-organizing process: A three-dimensional reaction, transport and mechanics model: Journal of Geophysical Research, v. 106, p. 803–818.

Tuncay, K., A. Park, and P. Ortoleva, 2000a, Sedimentary basin deformation: An incremental stress approach: Tectonophysics, v. 323, p. 77–104.

Tuncay, K., A. Park, and P. Ortoleva, 2000b, A forward fracture model to predict fracture orientation and properties: Journal of Geophysical Research, v. 105, p. 16719–16735.

Tuncay, K., A. Khalil, and P. Ortoleva, 2001, Failure, memory and cyclic fault movement: Bulletin of Seismological Society of America, v. 91, p. 538–552.

Ungerer, P., J. Burrus, B. Doligez, P. Y. Chénet, and F. Bessis, 1990, Basin evaluation by integrated two-dimensional modeling of heat transfer, fluid flow, hydrocarbon generation, and migration: AAPG Bulletin, v. 74, p. 309–335.

Van Keken, P. E., C. J. Spiers, A. P. van den Berg, and E. J. Muyzert, 1993, The effective viscosity of rocksalt: Implementation of steady-state creep laws in numerical models of salt diapirism: Tectonophysics, v. 225, p. 457–476.

Waite, M. E., S. Ge, H. Spetzler, and D. B. Bahr, 1998, The effect of surface geometry on fracture permeability: A case study using a sinusoidal fracture: Geophysical Research Letters, v. 25, p. 813–816.

Wang, C., and X. Xie, 1998, Hydrofracturing and episodic fluid flow in shale-rich basins— A numerical study: AAPG Bulletin, v. 82, p. 1857–1869.

Wang, J. S. Y., C. F. Tang, and R. A. Sternbentz, 1983, The state of the art of numerical modeling of thermo-hydrologic flow in fractured rock masses: Environmental Geology, v. 4, p. 133–199.

Wu, H. Q., and D. D. Pollard, 1995, An experimental study of the relationship between joint spacing and layer thickness: Journal of Structural Geology, v. 17, p. 887–905.

Zienkiewicz, O. C., and I. C. Cormeau, 1974, Visco-plasticity and creep in elastic solids— A unified numerical solution approach: International Journal for Numerical Methods for Engineering, v. 8, p. 821–845.